



**Pharmacodynamic Parameters  
(PDPs) of Human and Rat  
Acetylcholinesterase (AChE)  
Inhibition by Direct-Acting  
Organophosphorus (OP)  
Insecticides or Active Metabolites**

Prepared for

Dr. Nicole Zinn  
U.S. Environmental Protection Agency

Prepared by

Dr. Rudy J. Richardson  
University of Michigan

Dr. Richard Reiss  
Exponent

Original Version – June 30, 2017  
Revised – December 18, 2018

© Exponent, Inc.

1508118.000 - 5836

**STATEMENT OF NO DATA CONFIDENTIALITY CLAIMS**

No claim of confidentiality, on any basis whatsoever, is made for any information contained in this document. I acknowledge that information not designated as within the scope of FIFRA §10(d)(1)(A), (B), or (C) and which pertains to a registered or previously registered pesticide is not entitled to confidential treatment and may be released to the public, subject to the provisions regarding disclosure to multinational entities under FIFRA 10(g).

COMPANY:

Exponent

SUBMITTER:



12-18-2018

---

Richard Reiss

Date


Exponent


Principal Scientist & Group Vice President

STATEMENT OF COMPLIANCE WITH GOOD LABORATORY  
PRACTICE STANDARDS

This report is an update on *In vitro* acetylcholinesterase testing. Good Laboratory Practice Standards, 40 CFR Part 160, are not applicable to this submission.

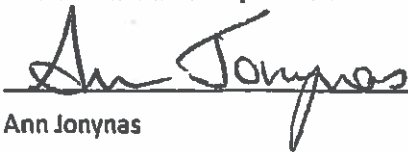
AUTHORS & SUBMITTER:

 12-18-2018  
\_\_\_\_\_  
Richard Reiss Date

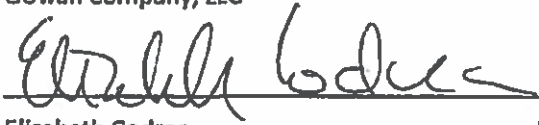
 12-18-2018  
\_\_\_\_\_  
Rudy Richardson Date

SPONSORS:

AMVAC Chemical Corporation

 18 December 2018  
\_\_\_\_\_  
Ann Jonynas Date

Gowan Company, LLC

 19 DEC 2018  
\_\_\_\_\_  
Elizabeth Codrea Date

FMC Corporation

 Dec 20, 2018  
\_\_\_\_\_  
Paul Whatling Date

# Contents

---

	<u>Page</u>
<b>List of Equations</b>	<b>6</b>
<b>List of Figures</b>	<b>7</b>
<b>List of Tables</b>	<b>8</b>
<b>Executive Summary</b>	<b>9</b>
<b>Introduction</b>	<b>11</b>
<b>Review of Prior Submissions</b>	<b>12</b>
<b>Study Hypotheses and Specific Aims</b>	<b>13</b>
Hypotheses	13
Hypothesis #1: Pharmacodynamic parameters for OP inhibition <i>in vitro</i> of erythrocyte (RBC) AChE can be used as a surrogate for pharmacodynamic parameters of brain AChE.	13
Hypothesis #2: Pharmacodynamic parameters for human and rat RBC AChE are expected to be similar.	13
Hypothesis # 3: Pharmacodynamic parameters of human or rat RBC AChE are not expected to vary with age, gender, or disease status.	13
Hypothesis #4: Pharmacodynamic parameters of human or rat AChE are not expected to vary with potential changes in posttranslational modification (PTM) associated with differences in age, gender, or disease status.	13
Hypothesis #5: Pharmacodynamic parameters of human or rat AChE are not expected to vary from potential mutations.	14
Corollaries	14
<b>Pharmacokinetics and Pharmacodynamics</b>	<b>15</b>
Pharmacokinetics	15
Pharmacodynamics	16
<b>AChE and OP Pesticide Mechanism and Mode of Action</b>	<b>18</b>
Cholinergic Synapses and the Physiological Function of AChE	18
Mechanism and Mode of Action of OP Inhibitors of AChE.	21
<b>PDPs for Inhibition of AChE by OP Compounds</b>	<b>25</b>
Kinetic and Equilibrium Constants	25
Determining $k_i$ under Pseudo-first-order Conditions	26
The $IC_{50}$ and $pIC_{50}$	28
Determining the $K_d$ and $k_2$ Components of $k_i$	30
Linear Transformations	31
Determining $K_d$ and $k_2$ in the Presence of Substrate	33

Literature Values for Paraoxon Inhibition of Rat and Human AChE	33
<b>Molecular Forms and Tissue Distribution of AChE</b>	<b>38</b>
<b>Intraspecies Sequence Homology of Brain and RBC AChE within Human or Rat</b>	<b>40</b>
<b>Interspecies Sequence Homology of Human and Rat AChE for Brain or RBC</b>	<b>43</b>
<b>Three-dimensional (3D) Structural Homology of Human and Rat AChE</b>	<b>46</b>
<b>Potential Intraspecies Variations in AChE PDPs</b>	<b>48</b>
<b>References</b>	<b>50</b>
<b>Appendix A. List of OP Compounds in the Experimental Program</b>	<b>59</b>

## List of Equations

---

	<u>Page</u>
<b>Eq. 1.</b> $K_d \cong k_{-1} / k_1$	<b>22</b>
<b>Eq. 2.</b> $k_i = k_2 / K_d$	<b>23</b>
<b>Eq. 3.</b> $\ln(v/v_o) = k_2[AB]t / ([AB] + K_d)$	<b>24</b>
<b>Eq. 4.</b> $\ln(\% \text{activity}) = -k't + \ln(100)$	<b>24</b>
<b>Eq. 5.</b> $\ln(\% \text{ activity}) = -k_i[AB]t + \ln(100)$	<b>24</b>
<b>Eq. 6.</b> $k' = k_i[AB]$	<b>24</b>
<b>Eq. 7.</b> $[AB]_{50} = IC_{50} = \ln(2) / k_i t \approx 0.693 / k_i t$	<b>25</b>
<b>Eq. 8.</b> $k' = \ln(v_o/v) / t = k_2 / (1 + K_d/[AB])$	<b>27</b>
<b>Eq. 9.</b> $1/k' = (k_2/[AB]K_d) + (1/k_2)$	<b>28</b>
<b>Eq. 10.</b> $[AB]/k' = [AB]/k_2 + K_d/k_2$	<b>29</b>
<b>Eq. 11.</b> $k' = -K_d k' / [AB] + k_2$	<b>29</b>
<b>Eq. 12.</b> $k' = k_2 / \{1 + (K_d/[AB])[1 + ([S]/K_m)]\}$	<b>30</b>

## List of Figures

---

	<u>Page</u>
Figure 1. Mammalian biotransformation of the OP insecticide, parathion.	12
Figure 2. Cholinergic synapses in the mammalian nervous system.	15
Figure 3. Neurochemistry of a mammalian cholinergic synapse.	16
Figure 4. Structures of acetylcholine(ACh) and analogs.	17
Figure 5. Inactivation of ACh by AChE.	18
Figure 6. Regeneration of Inhibited AChE by 2-PAM.	
Figure 7. Inhibition of AChE by an OP compound.	20
Figure 8. Simplified scheme for inhibition of AChE by an OP inhibitor.	23
Figure 9. Pseudo-first-order kinetics of hen brain microsomal AChE inhibition by chlorpyrifos methyl oxon (CPMO)	24
Figure 10. Direct determination of a fixed-time $plC_{50}$ .	26
Figure 11. Hyperbolic plot of $k'$ vs. $[AB]$ .	27
Figure 12. Lineweaver-Burk (double-reciprocal) plot.	28
Figure 13. Hanes-Woolf plot.	29
Figure 14. Eadie-Hofstee plot.	30
Figure 15. Literature values of inhibition constants for paraoxon inhibition of AChE.	32
Figure 16. AChE molecular forms.	35
Figure 17. Sequence alignment of human brain and human RBC AChE	38
Figure 18. Sequence alignment of rat brain and rat RBC AChE	39
Figure 19. Sequence alignment of human brain and rat brain AChE	41
Figure 20. Sequence alignment of human RBC and rat RBC AChE	42
Figure 21. 3D structure of human AChE	43
Figure 22. 3D homology model of rat AChE	44
Figure 23. 3D alignment of human and rat AChE	44

## List of Tables

---

	<u>Page</u>
Table 1. Inhibition Constants for Paraoxon against Human and Rat AChE.	34



## Executive Summary

---

This document provides a White Paper to supplement earlier submissions regarding a study to measure the kinetics of organophosphorus (OP) pesticide inhibition of acetylcholinesterase (AChE) for rat and humans and across different human life stages. The goal of the study is to quantify potential differences, if any, in AChE inhibition kinetics between rats and humans and across the human population. These results may be used to develop data-derived extrapolation factors (DDEFs) for interspecies and intraspecies pharmacodynamics.

The White Paper reviews the following hypotheses of the study:

- Hypothesis #1: Pharmacodynamic parameters for OP inhibition *in vitro* of erythrocyte (RBC) AChE can be used as a surrogate for pharmacodynamic parameters of brain AChE.
- Hypothesis #2: Pharmacodynamic parameters for human and rat RBC AChE are expected to be similar.
- Hypothesis #3: Pharmacodynamic parameters of human or rat RBC AChE are not expected to vary with age, gender, or disease status.
- Hypothesis #4: Pharmacodynamic parameters of human or rat AChE are not expected to vary with potential changes in posttranslational modification (PTM) associated with differences in age, gender, or disease status.
- Hypothesis #5: Pharmacodynamic parameters of human or rat AChE are not expected to vary from potential mutations.

Hypotheses #2 and #3 are directly tested through the experimental phase of the study (except the effect of disease status on intrahuman variability). Hypotheses #1, #4, and #5, and intrahuman variability related to disease status (part of Hypothesis #2) are addressed through a review of the literature and an analysis of the homology, sequence alignment, and 3D structural alignment of rat and human AChE.

The White Paper provides general background on relevant information, including detailed definitions of pharmacokinetics and pharmacodynamics, AChE and OP pesticide mechanism of action, and a mathematical exposition on the pharmacodynamic parameters for AChE inhibition by OP compounds. It explains why intrahuman variability in AChE activity levels does not affect the percent inhibition, which is the relevant parameter for risk assessment. Thus, intrahuman variability in AChE activity levels is not relevant for assessing pharmacodynamic uncertainty.

A review of the literature on AChE in rats and humans, together with an analysis of the homology, sequence alignment, and 3D alignment of rat and human AChE show the following:

- AChE in mammals is encoded by a single gene within each species, and the catalytic domains of the different molecular forms of AChE expressed in different tissues of rat and humans are identical within each species.
- The catalytic domains of brain and RBC AChE are identical within each species for rats and humans.
- The catalytic domains of rat and human AChE, while not identical, are highly similar. A comparison of the 3D alignment of rat and human AChE supports the hypothesis that rat and human AChE would be expected to interact similarly with OP inhibitors.
- Given that the amino acid sequence of the AChE catalytic domain determines its 3D structure, and the 3D structure of the catalytic domain determines the pharmacodynamic properties of the enzyme, variables that do not change the amino acid sequence, such as age, gender, and pregnancy, would not be expected to change the pharmacodynamic properties of the enzyme.
- While changes in posttranslational modifications (PTMs) of AChE associated with differences in age, gender, disease status, or genetics could potentially alter AChE structure, the only known PTM loci in human and rat AChE are N-glycosylation sites located on the protein surface far from the catalytic site. The literature shows that mutating these sites to prevent N-glycosylation had no significant effect on activity or pharmacodynamic parameters for ACh hydrolysis. In addition, elimination of the interchain disulfide bond or deletion of the C-terminal anchor domain had no effect on catalytic activity.
- Genetic mutations within the catalytic domain of AChE would be the only factor with the potential to alter intrinsic pharmacodynamic parameters of the enzyme. However, while the only known variant decreases thermal stability and the rate of inhibition by paraoxon *in vitro*, this mutation is extremely rare. The most frequent AChE variant is associated with the YT blood group antigen, and it has normal AChE activity.

All of these conclusions support the hypotheses that rat and human AChE inhibition kinetics parameters are substantially similar and that there is no significant intrahuman variability in AChE inhibition parameters. The review of the literature, together with AChE homology, sequence alignment, and 3D structural alignment, support these hypotheses. The proposed experimental program will test these hypotheses with a view toward informing judgments based on balanced assessments not only of statistical significance but also of biological importance (Lovell, 2013).

## Introduction

---

A consortium of three agrochemical manufacturers was formed, and a proposal was submitted to the U.S. Environmental Protection Agency (U.S. EPA) to perform testing on the inhibition kinetics of a series of organophosphorus (OP) pesticides from acetylcholinesterase (AChE) derived from erythrocytes (red blood cells, RBCs) of rats and humans. The consortium included AMVAC Chemical Corporation, Gowan Company, and FMC Corporation. A protocol was submitted to the U.S. EPA for review.

Briefly, the general outline of the study is as follows. AChE was derived from 6 rat sources (3 male and 3 female) and 18 human sources, including a mix of age, sex, and ethnicity. For a set of 17 OP pesticides or their active metabolites, inhibition kinetics parameters will be determined. Parameters include the bimolecular rate constant ( $k_i$ ), phosphorylation constant ( $k_p$ , also known as the acylation constant,  $k_2$ ), and dissociation constant ( $K_i$ , here denoted as  $K_d$  to distinguish it from the bimolecular rate constant,  $k_i$ , and the inhibition constant,  $K_i$ , used for reversible inhibitors). Paraoxon is also included in the program as a control given that its kinetic behavior is known. The other 17 OP compounds are direct-acting pesticides or active metabolites of the pesticides registered by the three companies. A list of the 17 OP compounds is included in Appendix A.

One hypothesis to be tested in the proposed study is that the inhibition kinetic parameters for rats and humans are essentially the same. Accordingly, the interspecies uncertainty factor for the pharmacodynamics of OP pesticides that exert their toxic effects via AChE inhibition could be modified from the default value of 3X. Furthermore, the program uses RBCs derived from a diverse population of 18 human subjects, including RBCs derived from cord blood, blood from juveniles, and blood from adults. Donors are from both sexes and different ethnicities. Data from these 18 subjects can be used to test the second hypothesis that there is no meaningful intraspecies variation in AChE inhibition. However, the U.S. EPA has raised recent concerns about the sufficiency of 18 human samples to represent potential intrahuman variability. As a supplemental line of evidence, this White Paper provides a literature review to determine if there are known intrahuman AChE differences that could influence OP inhibition pharmacodynamics. If the study demonstrates that there are no meaningful intraspecies differences in AChE inhibition, then the intraspecies pharmacodynamics uncertainty factor could be modified.

The purpose of this White Paper is to demonstrate that combining existing knowledge with new information to be generated by the proposed study will provide sufficient scientific understanding to permit a responsible modification in the interspecies and intraspecies pharmacodynamics uncertainty factors currently applied to AChE inhibition by direct-acting OP insecticides or active metabolites of OP insecticides. This goal is in accordance with National Academy of Sciences (NAS) and U.S. EPA guidelines on risk assessment, reference dose processes, use of data on cholinesterase inhibition, and interspecies/intraspecies extrapolations (NRC, 2009; U.S. EPA, 2014; U.S. EPA, 2016b).

## Review of Prior Submissions

---

The consortium submitted a preliminary experimental plan to the U.S. EPA on January 28, 2016, and met with the Agency to review the general concept of the study and experimental plan on January 3, 2016. The consortium submitted an updated experimental plan and protocol on August 17, 2016 (Exponent, 2016). The experimental plan and protocol was subsequently revised with two amendments that became effective on April 11, 2017 to expand the number of human blood samples to 18 and to increase the number of test compounds to 17 (18 including the reference compound, paraoxon) (Exponent, 2017a).

The U.S. EPA responded on November 16, 2016, with a review of the protocol (U.S. EPA, 2016a). The Agency concluded that the "... comparison of rat and human may apply (pending the conduct of the experiments and the Agency's review of their quality and sufficiency) to developing a data-derived inter-species extrapolation factor." Regarding the intraspecies factor, the U.S. EPA concluded, "... these data may apply (pending the conduct of the experiments and the Agency's review of their quality and sufficiency) to developing a data-derived intraspecies factor" ... "for some life stages (infants, children, men)." However, the reviewers noted, "... remaining concerns about the human dose-response for neurodevelopmental outcomes." The latter concerns were presumably related to the OP pesticide epidemiology literature and, in the U.S. EPA's opinion, preclude modifying the intraspecies factor for fetuses and pregnant women.

In its November 2016 review, the U.S. EPA also requested a response from the registrants on two issues. First, the Agency asked for the reasoning for selecting the chemicals proposed in the first protocol. This issue relates to the original study plan to test a diverse subset of OP pesticides and apply the result to the rest of the OP class. This issue is now moot because the current proposal calls for all OP compounds of interest to the consortium to be tested.

Second, the U.S. EPA asked for more justification for the sample size of 18 for the human samples. The consortium provided a memo on March 8, 2017 (Exponent, 2017b) that provided a detailed statistical analysis justifying the sample size.

## Study Hypotheses and Specific Aims

---

### Hypotheses

#### **Hypothesis #1: Pharmacodynamic parameters for OP inhibition *in vitro* of erythrocyte (RBC) AChE can be used as a surrogate for pharmacodynamic parameters of brain AChE**

Amino acid sequences (and therefore 3D structures) of the catalytic domains of brain and erythrocyte (RBC) AChE are identical within a given mammalian species, e.g., human or rat (Basova and Rozengart, 2009; Carr and Ollis, 2009; Cygler et al., 1993; Herkert et al., 2012; Uniprot, 2017a,b; Wiesner et al., 2007). The literature supporting this hypothesis is reviewed later in the report.

#### **Hypothesis #2: Pharmacodynamic parameters for human and rat RBC AChE are expected to be similar**

Catalytic domains of human and rat RBC AChE have high sequence identity (88.6%) and similarity (94.1%) as well as high predicted 3D structural homology (RMSD = 0.811 Å) (Geneious, 2017; Konagurthu et al., 2006; Uniprot 2017a,b; YASARA, 2017). The literature supporting the high sequence identity and structural similarity between rats and humans is reviewed later in the report, and this hypothesis is directly tested in the experimental phase of the study (except disease status).

#### **Hypothesis # 3: Pharmacodynamic parameters of human or rat RBC AChE are not expected to vary with age, gender, or disease status**

Age, gender, and disease status may change the levels but not the sequence of AChE throughout organ systems within an individual. Therefore, these factors would not be expected to alter the 3D structure of AChE (Massoulié et al., 2008). The literature supporting no meaningful age, gender, and disease state effect on the 3D structure of AChE is reviewed later in this report, and the hypothesis is directly tested in the experimental phase of the study.

#### **Hypothesis #4: Pharmacodynamic parameters of human or rat AChE are not expected to vary with potential changes in posttranslational modification (PTM) associated with differences in age, gender, or disease status**

Apart from four stable disulfide bonds (3 interchain; 1 interchain) and one glycerophosphatidylinositol (GPI) attachment site in the RBC anchor domain, there are three known PTM sites in human and rat AChE; all are N-glycosylation sites located on the protein surface far from the catalytic site (Uniprot,

2017a,b). Mutating these sites to prevent N-glycosylation had no significant effect on activity or pharmacodynamic parameters for ACh hydrolysis (Velan et al., 1993). Furthermore, elimination of the interchain disulfide bond or deletion of the C-terminal anchor domain had no effect on catalytic activity (Liang et al., 2009; Velan et al., 1991). The literature supporting this hypothesis is reviewed later in this report.

### **Hypothesis #5: Pharmacodynamic parameters of human or rat AChE are not expected to vary from potential mutations**

AChE mutations are extremely rare and those that do occur are not associated with disease or increased susceptibility to anti-AChE cholinergic toxicity (Bartels et al., 1993; Lockridge et al., 2016; Masson et al., 1994; Valle et al., 2011). The literature supporting this hypothesis is reviewed later in this report.

### **Corollaries**

- The extent to which pharmacodynamic parameters for OP inhibition of human and rat AChE agree will enable the pharmacodynamic component of the interspecies 10x uncertainty factor to be accordingly reduced (NRC, 2009; U.S. EPA, 2014).
- The extent to which age, gender, disease status, and genetics have no significant effect on the intrinsic pharmacodynamic parameters of human and rat AChE will enable the pharmacodynamic component of the intraspecies 10X uncertainty factor to be accordingly reduced (NRC, 2009; U.S. EPA, 2014).

## Pharmacokinetics and Pharmacodynamics

This section reviews definitions of pharmacokinetics and pharmacodynamics, which are important for understanding the experimental basis for the program and how the results apply to U.S. EPA risk assessments (U.S. EPA, 2000; 2002a-c; 2006; 2014).

### Pharmacokinetics

Pharmacokinetics (PK) refers to the effects that an organism has on a chemical to which it is exposed (Le, 2016). Because of its origins in pharmacology, PK is sometimes more narrowly confined to drugs (pharmaceutical or therapeutic agents). Similarly, in the context of toxicology, the term *toxicokinetics* (TK) refers to the effects that the organism has on a toxicant or toxin (Case, 1994). In the present document, PK will be used in the more global sense to apply to any exogenous substance (xenobiotic), although the focus will be on OP compounds that exert cholinergic neurotoxicity, such as the OP insecticide, parathion, and its active metabolite, paraoxon. Mammalian biotransformation pathways for parathion are shown in **Figure 1** (Mutch and Williams, 2006; Neal and Halpert, 1982).

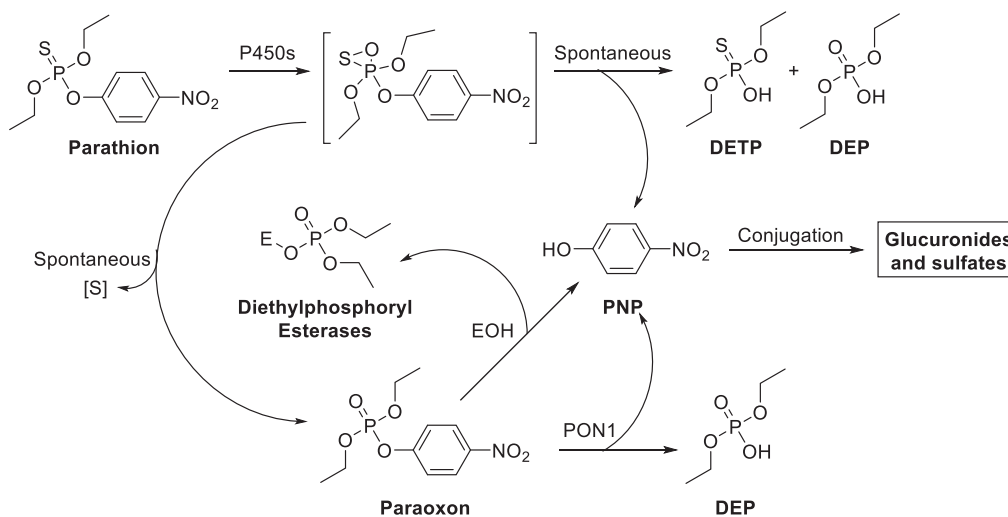


**Figure 1. Mammalian biotransformation of the OP insecticide, parathion.** Cytochromes P450 catalyze insertion of oxygen into the P-S double bond of parathion to form a reactive intermediate (square brackets). The intermediate can undergo two fates: (1) spontaneous hydrolysis to yield diethyl thiophosphate (DETP) or diethyl phosphate (DEP) and *p*-nitrophenol (PNP); or (2) spontaneous desulfuration to yield the active metabolite, paraoxon. DETP and DEP are water-soluble metabolites excreted in the urine; PNP is conjugated to form water-soluble glucuronides and/or sulfates that are excreted in the urine. Paraoxon reacts with serine esterases (EOH) to form covalent diethyl phosphoryl adducts with expulsion of the primary leaving group, PNP; it can also undergo hydrolysis catalyzed by paraoxonase-1 (PON1) to yield DEP and PNP (Mutch and Williams, 2006; Neal and Halpert, 1982).

PK encompasses the rates of absorption, distribution, metabolism (biotransformation), and excretion (ADME) of chemicals. Thus, it deals with the time-dependent locomotion (transport) and modification of foreign molecules by an organism. Mathematical descriptions of these processes are embodied in physiologically based pharmacokinetic (PBPK) models (Gearhart et al., 1990; Kuepfer et al., 2016).

PK factors determine the time course of achieving a given internal dose or concentration of a chemical or its active metabolite at a site of action (target site), such as an enzyme or receptor (Needham, 1994). In the case of parathion, if PK factors result in a critical concentration of the active metabolite, paraoxon, at the site of action, synaptic AChE, then cholinergic neurotoxicity will ensue. Conversely, if PK factors result in a subcritical concentration of paraoxon at synaptic AChE, then cholinergic neurotoxicity will not occur (Moretto, 1998; Thompson and Richardson, 2004).

Thus, by governing the time-dependent concentration of a chemical at its site of action, PK factors determine the intensity and duration of the biological response. However, PK factors do not determine the mechanism or mode of action of the biological response – these features occupy the domain of pharmacodynamics.

## Pharmacodynamics

Pharmacodynamics (PD) refers to the effects that a chemical has on an organism following a defined exposure (Farinde, 2016). Just as with PK, in the context of pharmacology, PD is sometimes narrowly confined to beneficial or therapeutic effects. Likewise, in toxicology, *toxicodynamics* (TD) has been used to refer to adverse or injurious effects (Voicu et al., 2009). In the present document, PD will be used generically to refer to given specified effects arising from a defined exposure; however, the focus will be on cholinergic neurotoxicity due to inhibition of AChE by OP compounds.

PD seeks to define the biological response elicited by a chemical stimulus and to reveal how the chemical brings about the response. Thus, the nature and cause of the biological response are derived from the molecular mechanism and consequent physiological mode of action of the chemical (Feimlee et al., 2012).

The mechanism of action underlying a biological response to a chemical begins with a molecular interaction between the chemical and a target, such as an enzyme or receptor. The effectiveness of the chemical-target interaction for a specific chemical to bring about a given biological response depends upon intrinsic characteristics of the target for binding to the chemical. Conversely, for a given target, the effectiveness of the chemical-target interaction for bringing about a biological response depends upon intrinsic properties of the chemical for binding to the target. Further physiological responses to a chemical-target interaction define the mode of action of the chemical that shapes the observed biological response in the intact organism (Gregus, 2013).



The following sections deal with the PD aspects of a particular biological response, cholinergic neurotoxicity, to a specific type of chemical, OP insecticides. It is assumed that the PK phase has successfully delivered an effective concentration of the active parent compound or active metabolite to the site of action, nervous system AChE. Therefore, the PD phase – the interactions of inhibitory OP compounds with AChE – can be studied in isolation without the need to consider the PK factors that were necessary to bring the active compound into contact with its biological target in sufficient quantity to elicit a biological response (Milesion et al., 1998; Mortensen et al., 1998; Thompson and Richardson, 2004).

## AChE and OP Pesticide Mechanism and Mode of Action

Before discussing the literature on potential differences, if any, in factors relevant to the pharmacodynamic parameters of interspecies (rat vs. human) or intrahuman variability, it is useful to review the function of AChE and OP pesticide mechanism and mode of action.

### Cholinergic Synapses and the Physiological Function of AChE

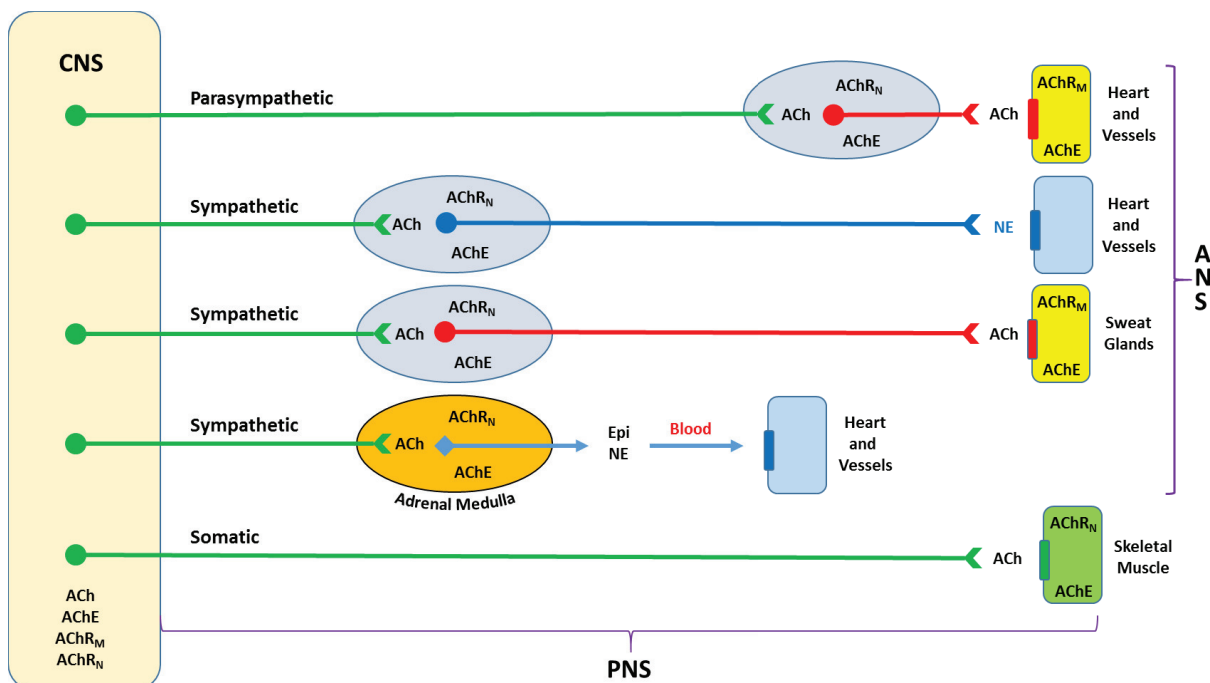


**Figure 2. Cholinergic synapses in the mammalian nervous system.** Neuron cell bodies are shown as filled circles: green = cholinergic preganglionic and cholinergic somatic; red = postganglionic cholinergic; blue = postganglionic adrenergic. Ganglia are depicted as blue-gray ovals. The adrenal medulla (orange oval) contains modified neurons (blue diamond) that secrete catecholamines (e.g., epinephrine (epi; adrenaline), norepinephrine (NE), and dopamine) into the blood. ACh = acetylcholine; AChE = acetylcholinesterase; AChR<sub>M</sub> = acetylcholine receptor, muscarinic; AChR<sub>N</sub> = acetylcholine receptor, nicotinic. ANS = autonomic nervous system (comprising the parasympathetic and sympathetic branches). CNS = central nervous system (brain and spinal cord). PNS = peripheral nervous system (peripheral nerves, ganglia, and synapses on neuroeffector organs, e.g., glands, smooth muscle, cardiac muscle, or skeletal muscle) (Weiner and Taylor, 1985).

In mammalian nervous systems, long-distance signals within a neuron are carried by electrical action potentials that travel along axons until they reach a synapse – a connection between two neurons or between a neuron and a target organ such as a gland or muscle. At the synapse, the electrical signal is transduced into a chemical signal mediated by a neurotransmitter. One such neurotransmitter is acetylcholine (ACh), which is widely employed in synapses throughout the central and peripheral

nervous systems (CNS and PNS, respectively). The connections that use ACh as the neurotransmitter are referred to as cholinergic synapses (Holz and Fisher, 2012).

**Figure 2** illustrates the ubiquity of cholinergic synapses in mammals, showing that these connections are involved in neurotransmission in the CNS (brain and spinal cord) and PNS, which includes the somatic nervous system (controlling voluntary muscles) and autonomic nervous system (ANS). The ANS includes the sympathetic and parasympathetic nervous systems that govern functions of glands, smooth muscle, or cardiac muscle in the various internal organs (Weiner and Taylor, 1985).

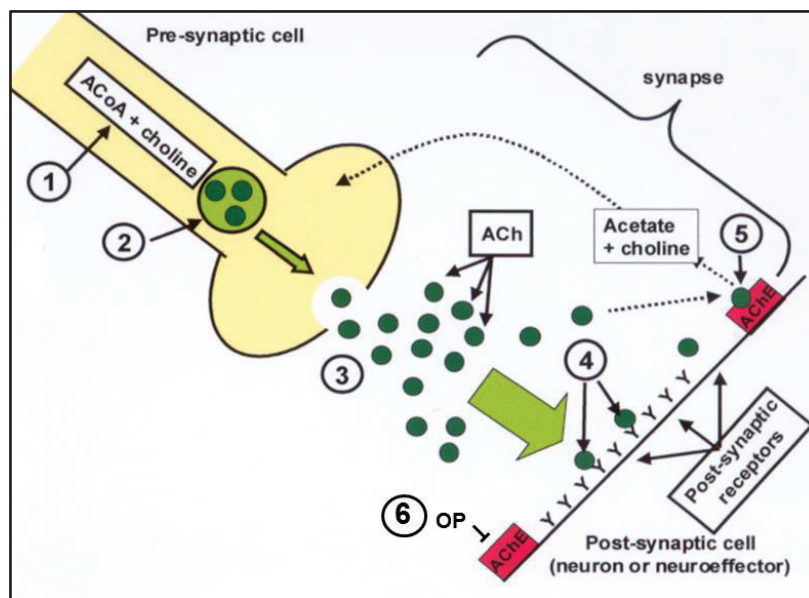


**Figure 3. Neurochemistry of a mammalian cholinergic synapse.** The cholinergic synapse consists of the axonal ending of the presynaptic neuron, a gap (synaptic cleft) between the presynaptic membrane and the plasma membrane of the postsynaptic cell (e.g., another neuron, a glandular cell, or a smooth or striated muscle cell). Steps depicted in the operation of the cholinergic synapse: 1 = synthesis of acetylcholine (ACh) from acetyl coenzyme A (ACoA) and choline; 2 = packaging of ACh into synaptic vesicles for storage; 3 = movement of synaptic vesicles to presynaptic membrane, fusion with the membrane, and release of ACh into the synaptic cleft; 4 = binding of ACh to ACh receptors on the postsynaptic membrane; 5 = inactivation of AChE via hydrolysis catalyzed by acetylcholinesterase (AChE) -- the products acetate and choline are taken up by the presynaptic cell to be recycled into new ACh molecules; 6 = inhibition of AChE by a direct-acting organophosphorus (OP) insecticide or active metabolite – ACh cannot be inactivated, resulting in prolonged hyperstimulation of ACh receptors and eventual fatigue of response in the postsynaptic cell (Holz and Fisher, 2012).

The five essential steps in the tightly regulated operation of a chemical synapse – in particular, the cholinergic synapse – are shown in **Figure 3**. As in all chemical synapses, the neurotransmitter (ACh in this case) must be synthesized (1) and packaged into synaptic vesicles for storage until needed (2). Upon arrival of an electrical action potential at the synapse, synaptic vesicles move to the presynaptic membrane, fuse with the membrane, and release their contents of ACh into the synaptic cleft (3). The neurotransmitter then diffuses across the synaptic cleft and binds to receptor molecules on the plasma

membrane of the target cell, thereby triggering events that lead to a physiological response (4). ACh is inactivated by AChE (5).

The category of physiological response elicited by the neurotransmitter depends on the class and subtype of receptor. For example, members of the class of nicotinic ACh receptors (so named because they respond to nicotine) comprise ligand-gated ion channels that open the channel resulting in depolarization of the postsynaptic cell – an excitatory response. In contrast, members of the class of muscarinic ACh receptors (so named because they respond to muscarine) are metabotropic G-protein-coupled receptors. The structures of muscarine and nicotine in comparison with ACh and the muscarinic antagonist atropine are shown in **Figure 4** (Fisher and Wonnacott, 2012).

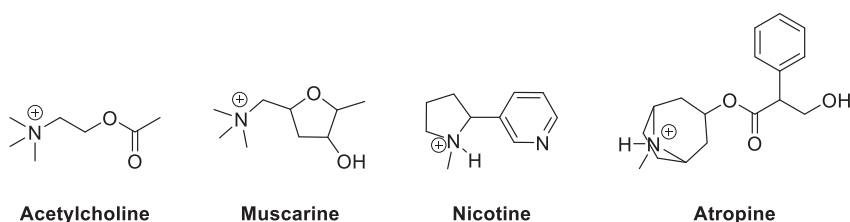


**Figure 4. Structures of acetylcholine (ACh) and analogs.** Muscarine and nicotine are the prototypic agonists of muscarinic and nicotinic ACh receptors, respectively. Atropine is a competitive antagonist of ACh on muscarinic receptors (Fisher and Wonnacott, 2012).

Depending upon the subtype of muscarinic receptor, its interaction with ACh can produce either depolarization (excitation) or hyperpolarization (inhibition). In any case, regardless of receptor class or subtype, the neurotransmitter can be thought of as a molecular switch that turns on a physiological response – either excitation or inhibition. As with any regulated physiological system, whenever there is a switch for turning a process on, there must also be a switch for turning it off. The off-switch in a cholinergic synapse is the enzyme, AChE (**Figure 3**, step 5) (Fisher and Wonnacott, 2012).

Thus, the physiological function of AChE in mammals, including rats and humans, is to terminate the action of ACh as a neurotransmitter in cholinergic synapses. AChE accomplishes its function by catalyzing the hydrolysis of ACh into acetate and choline, which are then taken up by the presynaptic neuron where they can be recycled to produce new ACh molecules (Thompson and Richardson, 2004).

AChE is also found on the surface of mammalian erythrocytes (red blood cells, RBCs) at varying levels of activity depending upon species. Humans have the highest RBC AChE activity. On a relative percent scale setting humans at 100%, RBC AChE activity in rats is 12% and only 0-2% in cats (Herz and Kaplan, 1973; Lev-Lehman et al., 1997). The physiological function of catalytically active AChE on RBCs remains unknown, although in humans the AChE protein serves as the YT blood group antigen (Bartels et al., 1993).

The reactions and associated kinetic constants for the enzymatic hydrolysis of ACh by AChE are shown in **Figure 5**.

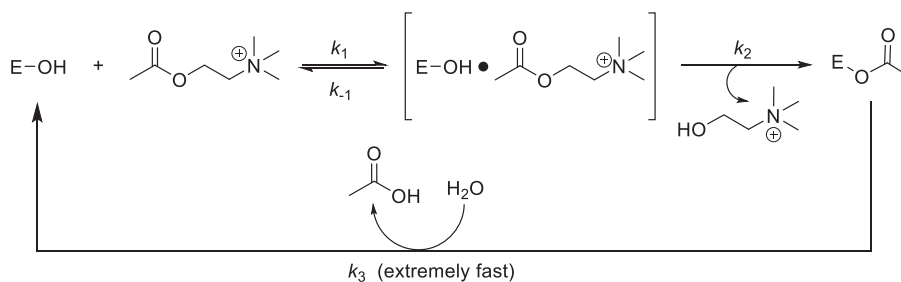


**Figure 5. Inactivation of Acetylcholine (ACh) by AChE.** Enzyme-catalyzed hydrolysis of the natural substrate, acetylcholine (ACh), by acetylcholinesterase (AChE, depicted as E-OH to emphasize the role of the activated serine hydroxyl group in the active site).  $k_1$  = second-order rate constant for formation of the Michaelis complex (shown in square brackets).  $k_{-1}$  = first-order rate constant for decomposition of the Michaelis complex back into E-OH and ACh.  $k_2$  = first-order rate constant for formation of acylated (acetylated) enzyme and choline from the Michaelis complex.  $k_3$  = pseudo-first-order rate constant ( $\text{H}_2\text{O}$  in excess) for extremely rapid hydrolysis of acylated (acetylated) enzyme to yield acetic acid and regenerated enzyme, thus completing the catalytic cycle and inactivating ACh as a neurotransmitter (Thompson and Richardson, 2004).

As shown in **Figure 5**, AChE and its substrate ACh interact to form a reversible Michaelis complex. The complex has two possible fates: (1) it can revert to the initial reactants; or (2) the planar carbonyl carbon atom of the substrate can undergo nucleophilic attack by the active site serine hydroxyl group of the enzyme to form a tetrahedral transition state that collapses into the acylated enzyme with expulsion of choline. The acylated enzyme is exceedingly short-lived, because it is hydrolytically deacylated (specifically, deacetylated) at an extremely rapid rate to yield acetic acid and regenerated enzyme. This concerted acylation and deacylation of the AChE active site constitute a highly efficient catalytic cycle that rapidly hydrolyzes the substrate, ACh, into acetic acid and choline, thereby inactivating the neurotransmitter (Thompson and Richardson, 2004).

## Mechanism and Mode of Action of OP Inhibitors of AChE

A potential sixth step that can occur in the neurochemistry of cholinergic synapses is the inhibition of AChE by an exogenous organophosphorus (OP) compound, such as a direct-acting OP insecticide or an active metabolite of an OP insecticide (**Figure 3**, step 6) (Richardson, 2010).

Biological systems usually have considerable reserve capacity. With respect to AChE, heterozygous AChE (+/-) knockout mice are apparently healthy despite the fact that they have about 50% of the control levels of brain AChE activity (Xie et al., 2000). In addition, the threshold level of AChE inhibition for clinical signs of cholinergic toxicity is approximately 50% (Moretto, 1998). Thus, it would appear that normal cholinergic synapses contain approximately twice the amount of AChE needed for ordinary

function. Inhibiting a sufficient amount of the enzyme beyond the ~50% threshold inactivates the off-switch of the cholinergic synapse, thus jamming it in the always-on position until AChE is restored to above ~50% activity by reactivation of inhibited AChE and/or resynthesis of new AChE molecules.

Without a sufficient level of active AChE, cholinergic signals cannot be shut off. As more electrical action potentials from cholinergic neurons throughout the nervous system arrive at their terminals, more synapses are activated, compounding the consequent physiological responses in the target cells. Moreover, even without the arrival of action potentials, there is always a slow leak of ACh into the synaptic cleft, producing a background level of activated postsynaptic receptors. Regardless of the mechanism whereby ACh is released into the synaptic cleft, without enough active AChE to inactivate it, the neurotransmitter quickly reaches critical levels for activating postsynaptic receptors (Fisher and Wonnacott, 2012; Thompson and Richardson, 2004).

Because of the widespread distribution of cholinergic synapses in the body as shown in **Figure 2**, virtually all glands, smooth muscles, cardiac muscles, and skeletal muscles are affected by a suprathreshold exposure to an OP inhibitor of AChE. The net effects in the intact organism include involuntary salivation, lacrimation (tearing), urination, and defecation (SLUD) along with muscle twitching and fasciculations. Heart rate is often slowed (bradycardia), but it can also be increased (tachycardia), depending upon the balance between parasympathetic and sympathetic effects. There is concomitant hypersecretion of mucus in the airways, impairing the flow of oxygen. Ultimately, synapses of somatic muscle (neuromuscular junctions) undergo fatigue, resulting in paralysis. Muscle paralysis includes the diaphragm and intercostal muscles that ventilate the lungs, further compromising oxygen delivery to tissues. In the CNS, effects of high levels of AChE inhibition include convulsions and respiratory paralysis progressing to coma and death (Richardson, 2010; Thompson and Richardson, 2004).

Fortunately, understanding the details of the mechanism and mode of action of OP insecticide poisoning has led to the development of effective antidotes. First, atropine, a competitive antagonist of ACh at muscarinic receptors (**Figure 4**) is given to counteract the muscarinic effects of excess ACh. Second, a powerful nucleophile such as the oxime, 2-pyridine aldoxime methyl iodide (2-PAM), is given to reactivate inhibited AChE (**Figure 6**). An anticonvulsant such as the benzodiazepine, diazepam, can also be administered to counteract convulsions (Thompson and Richardson, 2004).

The reactions and associated rate constants for the inhibition of AChE by an OP compound (paraoxon, the active metabolite of the OP insecticide, parathion) are shown in **Figure 7**. AChE and the OP inhibitor, paraoxon, interact to form a reversible Michaelis-type complex, analogous to the initial encounter of AChE with its physiological substrate, ACh. The Michaelis-type complex has two possible fates: (1) it can revert to the initial reactants; or (2) the tetrahedral phosphoryl phosphorus atom of the inhibitor can undergo nucleophilic attack by the active site serine hydroxyl group of the enzyme to form

a trigonal bipyramidal transition state that collapses into the acylated (organophosphorylated) enzyme with expulsion of the primary leaving group, *p*-nitrophenol (Richardson et al., 2015).

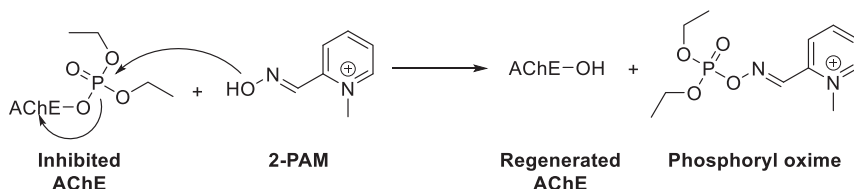


**Figure 6. Regeneration of Inhibited AChE by 2-PAM.** Acetylcholinesterase (AChE) inhibited by a diethyl phosphate (e.g., paraoxon) is regenerated by the oxime, 2-pyridine aldoxime methyl iodide (2-PAM) (iodide counterion not shown). The oxime acts as a potent nucleophile that attacks the phosphorus atom of the diethyl phosphoryl moiety, displacing AChE as the leaving group and forming a phosphoryl oxime (Thompson and Richardson, 2004).

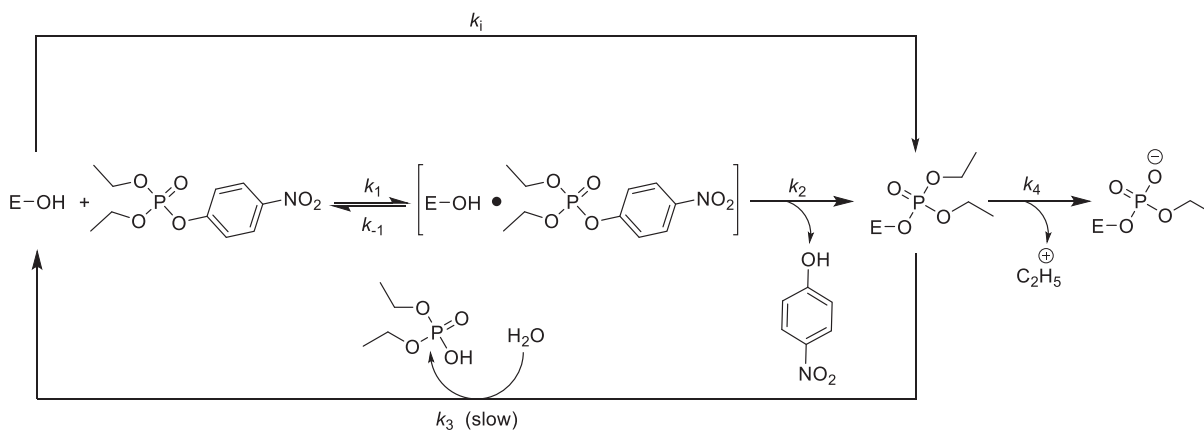


**Figure 7. Inhibition of AChE by an OP compound.** AChE is depicted as E-OH to emphasize the role of the activated serine hydroxyl group in the active site of the enzyme. To provide a specific example, the OP inhibitor is paraoxon, the active metabolite of the insecticide, parathion.  $k_1$  = second-order rate constant for formation of the Michaelis-type complex (shown in square brackets).  $k_{-1}$  = first-order rate constant for decomposition of the Michaelis-type complex back into E-OH and paraoxon.  $k_2$  = first-order rate constant for formation of acylated (organophosphorylated) enzyme with expulsion of the *p*-nitrophenol primary leaving group from the Michaelis-type complex.  $k_3$  = pseudo-first-order rate constant ( $H_2O$  in excess) for the slow hydrolysis of acylated enzyme to yield diethyl phosphate and regenerated enzyme.  $k_4$  = first-order rate constant for the “aging” reaction, involving net loss of an ethyl group from the organophosphorylated enzyme to yield a negatively charged monoethylphosphoryl moiety covalently attached to the active site of the enzyme.  $k_i$  = overall bimolecular (second-order) rate constant of inhibition (Richardson et al., 2015).

Unlike acetylated AChE that transiently formed by acylation of the enzyme by its physiological substrate, organophosphorylated AChE is relatively long-lived, because its rate of hydrolysis is many orders of magnitude slower than that of the acetylated enzyme. Thus, the organophosphorylated AChE is inhibited – the active site is blocked, and the enzyme is thereby prevented from processing its normal substrate, ACh (Richardson, 2010).

Moreover, whereas the acetylated enzyme formed during the processing of ACh by AChE can only undergo hydrolysis to yield regenerated enzyme, the organophosphorylated enzyme can undergo an alternative reaction (aging) to yield a negatively charged monoethylphosphoryl moiety covalently bound to the active site serine of the enzyme. The aged enzyme is still inhibited; furthermore, it is locked in the aged-inhibited state and cannot be reactivated, even by powerful nucleophiles such as certain oximes (e.g., 2-PAM) that can reactivate the inhibited enzyme before aging takes place (**Figure 6**) (Thompson and Richardson, 2004).

Thus, the mechanism of action of a cholinergic neurotoxic OP insecticide or active metabolite is to inhibit AChE by mimicking the substrate, ACh. The OP compound behaves as an inhibitor rather than a substrate because the rate of reactivation of the acylated enzyme is much slower for the OP compound than it is for the physiological substrate, ACh. In addition, in the case of the OP compound, the acylated enzyme can undergo an aging reaction to lock the inhibitor in place, rendering it incapable of being reactivated, even by powerful nucleophiles such as oximes (Milesion et al., 1998; Richardson et al., 2015).

Furthermore, the mode of action of a cholinergic neurotoxic OP insecticide stems from the fact that inhibited AChE cannot inactivate ACh to terminate its action as a neurotransmitter. The result is poisoning by excess ACh in cholinergic synapses throughout the nervous system (cholinergic neurotoxicity), resulting in hyperstimulation followed by fatigue of ACh receptors (Milesion et al., 1998; Thompson and Richardson, 2004).

The rate and equilibrium constants characterizing individual steps in the interaction of OP inhibitors with AChE constitute the pharmacodynamic parameters (PDPs) described in detail in the next section.



## PDPs for Inhibition of AChE by OP Compounds

---

Rate and equilibrium constants associated with the reactions shown in **Figure 7** can be measured experimentally using *in vitro* enzyme assays, thus yielding quantitative PDPs for the inhibition, reactivation, and aging of AChE by an OP compound (Clothier et al., 1981).

Here, the focus is on the steps involved in inhibition rather than the postinhibitory steps of reactivation ( $k_3$ ) and aging ( $k_4$ ). This is because the  $k_3$  and  $k_4$  values for OP compounds with the same dialkylphosphoryl moiety (e.g., all diethyl phosphates) would be expected to be identical, although relatively small differences have been observed (Carr and Chambers, 1996). On the other hand, rate constants for inhibition of AChE by direct-acting OP insecticides or active metabolites can differ by orders of magnitude owing to the structural diversity afforded by various primary leaving groups (Main, 1980).

The mathematical relationships describing the kinetics of irreversible inhibition of AChE and other serine esterases by OP compounds summarized here have been elegantly set forth in the classic work by Aldridge and Reiner (1972), and synopses are available in other sources (Clothier et al., 1981; Main, 1980; Richardson, 1992; Richardson et al., 2015). The equations featured below provide a basic and generalizable foundation for determining the inhibitory potency of OP compounds and other acylating inhibitors against AChE and other serine hydrolases. For complex scenarios beyond the scope of this White Paper, other equations have been developed (Estevez and Vilanova, 2009).

### Kinetic and Equilibrium Constants

Considering only the steps involved in forming the acylated (phosphorylated) enzyme, **Figure 7** can be simplified as shown in **Figure 8**. This simplification is reasonable for most OP inhibitors of AChE, because  $k_3$  and  $k_4$  are often orders of magnitude smaller than  $k_2$ . In addition,  $k_2$  is usually much smaller than  $k_{-1}$ , so that the equilibrium constant,  $K_d$ , for the dissociation of the Michaelis-type complex,  $E \bullet AB$ , is approximately given by **Eq. 1**:

$$K_d \cong k_{-1} / k_1 \tag{Eq. 1}$$

The nomenclature followed here is that equilibrium constants are presented as upper-case italicized “ $K$ ” with a subscript, such as “ $d$ ” indicating “dissociation”. Rate constants are presented as lower-case italicized “ $k$ ” with a subscript such as “ $-1$ ” indicating the first reverse reaction in a given sequence. In addition, unless noted otherwise, concentrations are in molar units ( $M$ ) and time is in minutes (min). Given that  $k_{-1}$  is a first-order rate constant that has units of inverse time, e.g.,  $\text{min}^{-1}$ , and  $k_1$  is a second-order rate constant with units of  $M^{-1}\text{min}^{-1}$ ,  $K_d$  is a Michaelis-type equilibrium constant in molar

units that represents the concentration required to achieve 50% of the maximum rate of production of the acylated (phosphorylated) enzyme.  $K_d$  is also regarded as a measure of the affinity of an OP inhibitor for binding to the active site of the enzyme. Thus, low values of  $K_d$  correspond to high affinity, and high values of  $K_d$  correspond to low affinity (Richardson et al., 2015).

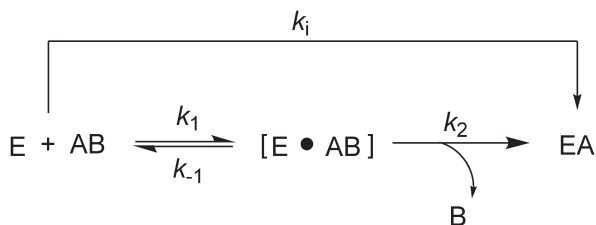


**Figure 8. Simplified scheme for inhibition of AChE by an OP inhibitor.** E = AChE, AB = OP inhibitor, A = acylating (phosphorylating) component, B = primary leaving group. The Michaelis-type reversible complex is shown within square brackets. EA = acylated (phosphorylated) inhibited enzyme.  $k_1$  = second-order rate constant for formation of the reversible complex;  $k_{-1}$  = first-order rate constant for dissociation of the reversible complex;  $k_2$  = first-order acylation (phosphorylation) rate constant for formation of the acylated (phosphorylated) inhibited enzyme with expulsion of the primary leaving group, B.  $k_i$  = overall second-order (bimolecular) rate constant of inhibition for formation of the inhibited enzyme from the enzyme and inhibitor. This scheme omits reactivation ( $k_3$ ) and aging ( $k_4$ ), which are usually orders of magnitude slower than phosphorylation ( $k_2$ ) (Main, 1980).

The overall progress of the reaction from enzyme (E) and inhibitor (AB) to phosphorylated (inhibited) enzyme (EA) with expulsion of the primary leaving group (B) is characterized by the bimolecular rate constant of inhibition,  $k_i$ . This important measure of inhibitory potency is determined by measuring the activity remaining as a function of time of preincubation of the enzyme with various concentrations of inhibitor, where  $[\text{AB}] > 10[\text{E}]$ . The substrate (ACh when E = AChE) is added after the preincubation interval for a further incubation period to determine the activity remaining after inhibition (Richardson, 1992; Richardson et al., 2015). When  $[\text{AB}] \ll K_d$ ,  $k_i$  is given by **Eq. 2**:

$$k_i = k_2 / K_d \quad \text{(Eq. 2)}$$

It is important to note that  $k_i$  is a composite of the acylation (phosphorylation) rate constant (sometimes written as  $k_p$ ) with units of  $\text{min}^{-1}$  and the dissociation equilibrium constant,  $K_d$ , with units of  $M$ . Therefore,  $k_i$  has the units of a second-order (bimolecular) rate constant,  $M^{-1}\text{min}^{-1}$ .

## Determining $k_i$ under Pseudo-first-order Conditions

Pseudo-first-order inhibition kinetics are obtained under the commonly observed conditions when the concentration of the Michaelis-type enzyme-inhibitor complex  $[\text{E} \bullet \text{AB}]$  is low,  $k_2$  is high,  $k_3 \ll k_2$ , and  $[\text{AB}] > 10[\text{E}]$ , where  $[\text{E}]$  = the concentration of native enzyme (Richardson et al., 2015). In such cases, **Eq. 3** applies:

$$\ln(v/v_0) = k_2[AB]t/([AB] + K_d) \quad (\text{Eq. 3})$$

In **Eq. 3**,  $v$  is the velocity (rate) of enzymatic hydrolysis of its substrate (i.e., ACh for AChE) at time =  $t$ , and  $v_0$  is the rate at time zero. Substituting (% activity/100) for  $(v/v_0)$ , letting  $k' = k_2[AB]/([AB] + K_a)$ , and rearranging yields **Eq. 4**:

$$\ln(\% \text{activity}) = -k't + \ln(100) \quad (\text{Eq. 4})$$

Thus, plots of  $\ln(\% \text{ activity})$  versus  $t$  ("primary kinetic plots") will be straight lines with slopes =  $-k'$  and y-intercept =  $\ln(100) \approx 4.605$ , as shown in **Figure 9A**.

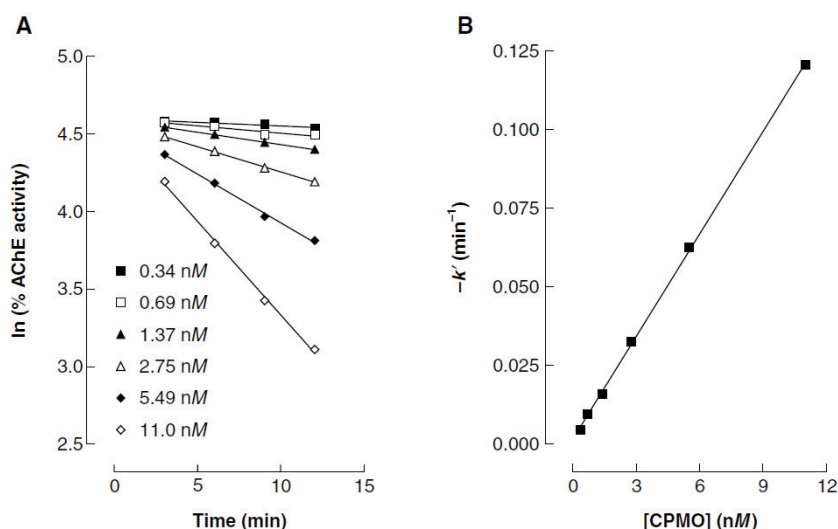


**Figure 9. Pseudo-first-order kinetics of hen brain microsomal AChE inhibition by chlorpyrifos methyl oxon (CPMO).** **A.** Primary kinetic plots of  $\ln(\% \text{ AChE activity})$  vs. time of preincubation with various concentrations of the OP inhibitor, CPMO. **B.** Secondary plot of first-order rate constants  $k'$  (slopes of the primary plots in panel **A**) vs. inhibitor concentration. The slope of the secondary plot is the bimolecular rate constant of inhibition,  $k_i = 10.9 \pm 0.1 \mu\text{M}^{-1}\text{min}^{-1}$ , corresponding to a 20-min  $\text{IC}_{50}$  of  $3.18 \pm 0.03 \text{ nM}$  (pH 7.6 phosphate, 37 °C) (Kropp and Richardson, 2003).

In addition, the experimentally determined dependence of  $\ln(\% \text{ activity})$  on the preincubation time ( $t$ ) and inhibitor concentration  $[AB]$  is given by **Eq. 5**:

$$\ln(\% \text{ activity}) = -k_i[AB]t + \ln(100) \quad (\text{Eq. 5})$$

Setting **Eq. 4** and **Eq. 5** equal to each other gives **Eq. 6**:

$$k' = k_i[AB] \quad (\text{Eq. 6})$$

Therefore, a plot of  $-k'$  versus  $[AB]$  (“secondary plot”) will yield a straight line with slope =  $k_i$ , as shown in **Figure 9B**. The  $k_i$  value thus obtained is an indication of the overall inhibitory potency of a given compound (such as a direct-acting OP inhibitor) against a particular serine hydrolase (such as AChE). However, it is important to realize, as shown in **Eq. 2**, that  $k_i$  is a composite quantity that includes  $K_d$ , an indication of the affinity of the inhibitor for the enzyme, and  $k_2$ , the rate of organophosphorylation of the enzyme by the inhibitor. Inspection of **Eq. 2** and **Eq. 5** shows that the units of  $k_i$  are  $[AB]^{-1}t^{-1}$ . For example, the  $k_i$  obtained for chlorpyrifos methyl oxon (CPMO) against hen brain microsomal AChE in pH 7.6 phosphate buffer at 37°C is  $10.9 \pm 0.1 \mu\text{M}^{-1}\text{min}^{-1}$  (Kropp and Richardson, 2003).

## The $IC_{50}$ and $pIC_{50}$

An especially useful relationship is provided by substituting a percent activity of interest into **Eq. 5** to yield the inhibitor concentration at a given time of preincubation with enzyme that would yield the particular percent activity. For example, when  $[AB]_{50} = IC_{50}$  = the inhibitor concentration required to produce 50% inhibition of the enzyme at a given time,  $t$ , of preincubation of enzyme and inhibitor at defined conditions of pH, temperature, and ionic strength before adding substrate, we have **Eq. 7**:

$$[AB]_{50} = IC_{50} = \ln(2)/k_i t \approx 0.693/k_i t \quad (\text{Eq. 7})$$

Note from **Eq. 7** that  $k_i$  and  $IC_{50}$  are reciprocally related, and that  $IC_{50}$  is time dependent (Richardson et al., 2015).

It is valid to calculate an  $IC_{50}$  from a  $k_i$  value when pseudo-first-order kinetic behavior is observed. However, it is not valid to calculate a  $k_i$  from an experimentally determined fixed-time  $IC_{50}$ , because the  $IC_{50}$  alone contains no information about the kinetic behavior of the inhibition reaction (Richardson et al., 2015).

In addition, if inhibitory potency is assessed by measuring fixed-time  $IC_{50}$  values directly, it is essential to report the time of preincubation along with the concentration, because the  $IC_{50}$  decreases as the preincubation time increases (Aldridge and Reiner, 1972; Clothier *et al.*, 1981; Richardson, 1992; Richardson et al., 2015).

For example, using **Eq. 7**, the 20-min  $IC_{50}$  for CPMO against hen brain microsomal AChE at pH 7.6 and 37°C may be calculated from the  $k_i$  given above to be  $0.693/[(10.9 \mu\text{M}^{-1}\text{min}^{-1})(20 \text{ min})] = 0.00318 \mu\text{M} = 3.18 \text{ nM}$  (Kropp and Richardson, 2003).

Like the bimolecular rate constant of inhibition,  $k_i$ , the  $IC_{50}$  is a measure of inhibitory potency, but reciprocally related. Inhibitory potency is directly related to the  $k_i$  – larger values reflect greater potency, but inversely related to the  $IC_{50}$  – smaller values reflect greater potency. Although it is

preferable to assess inhibitory potency of an OP compound against AChE kinetically rather than by determining fixed-time  $IC_{50}$  values (Kropp and Richardson, 2003; Mortensen et al., 1998; Strelow, 2017), the latter can be easier to conceptualize (Thompson and Richardson, 2004).

Quite often,  $IC_{50}$  values are expressed as  $-\log IC_{50} = pIC_{50}$  after converting the  $IC_{50}$  to  $M$  units. For example,  $IC_{50} = 3.18 \text{ nM} = 3.18 \times 10^{-9} \text{ M}$ ;  $-\log(3.18 \times 10^{-9}) = pIC_{50} = 8.50$ . The  $pIC_{50}$  has some advantages over the  $IC_{50}$  (Elkins et al., 2013; Navre, 2015). For example, it is less cumbersome to present  $pIC_{50}$  data as opposed to  $IC_{50}$  values, which require exponents. Moreover,  $pIC_{50}$  values are more intuitive than  $IC_{50}$  data for conveying the relative strength of inhibitors. Like the  $k_i$ , the  $pIC_{50}$  is directly related to inhibitory potency – the larger the  $pIC_{50}$ , the more potent is the inhibitor. In addition, when concentrations are equally spaced on a log scale, confidence intervals and standard errors for the  $pIC_{50}$  will be symmetrical on a log scale (GraphPad, 2018a).

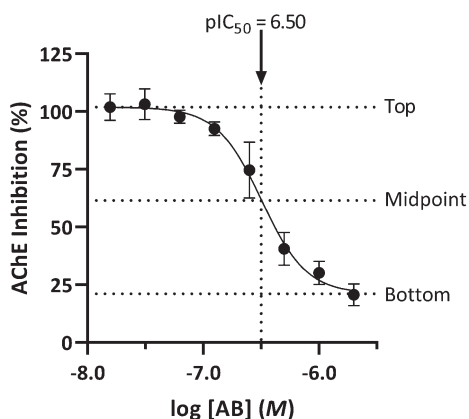


**Figure 10. Direct determination of a fixed-time  $pIC_{50}$ .** Hypothetical data for % inhibition of AChE produced by a 20-min preincubation of the enzyme with varying concentrations of inhibitor (AB). Nonlinear regression of the sigmoid curve is used to estimate upper and lower plateaus and the midpoint between them from which the relative 20-min  $pIC_{50}$  of 6.50 and 95% CI of 6.41 to 6.58 are obtained (GraphPad, 2018a).

**Figure 10** illustrates a hypothetical example of the experimental determination of a fixed-time (20-min)  $pIC_{50}$  for inhibition of AChE. A plot of % inhibition of AChE activity vs. log (inhibitor concentration) typically produces a sigmoid curve for which upper and lower plateaus can be estimated using nonlinear regression. A line parallel to the concentration axis midway between the plateaus crosses the sigmoid curve thus defining the 50% relative response. The negative log concentration corresponding to the 50% relative response is the  $pIC_{50}$ . In this example, nonlinear regression yields a 20-min  $pIC_{50}$  value of 6.50 with a 95% CI of 6.41 to 6.58. The corresponding value for the 20-min  $IC_{50}$  is  $3.16 \times 10^{-7} \text{ M}$ , with a 95% CI of  $2.63 \times 10^{-7} \text{ M}$  to  $3.89 \times 10^{-7} \text{ M}$ . Note that in this method, the 50% point does not necessarily coincide with 50% on the percent inhibition axis (GraphPad, 2018b). It is also important to realize that although the 95% CI is nearly symmetrical for the  $pIC_{50}$ , it will generally be highly asymmetrical for the

IC<sub>50</sub>. Moreover, whereas it is possible to compute the standard error of the mean (SEM) for the pIC<sub>50</sub>, the antilog of this value is not the SEM of the IC<sub>50</sub>.

Overall, when considering indicators of potency for irreversible inhibitors of AChE, it is preferable to use pIC<sub>50</sub> rather than IC<sub>50</sub> as a fixed-time parameter, and the kinetically determined bimolecular rate constant of inhibition,  $k_i$ , is preferable to either fixed-time quantity.

## Determining the $K_d$ and $k_2$ components of $k_i$

Under certain conditions, it is possible to determine the  $K_d$  and  $k_2$  components of  $k_i$  separately. For example, if the secondary plot is not linear, or if the primary kinetic plots do not pass through the origin (ln(100)), these are indications of an appreciable concentration of a Michaelis-type complex. In such cases, the  $K_d$  term must be explicitly included. Combining **Eq. 3** and **Eq. 4** yields **Eq. 8**:

$$k' = \ln(v_0/v)/t = k_2/(1 + K_d/[AB]) \quad (\text{Eq. 8})$$

**Eq. 8** has exactly the same form as the classic Michaelis-Menten equation describing the kinetics of an enzyme-substrate reaction. Accordingly, a plot of  $k'$  vs.  $[AB]$  is a rectangular hyperbola, as shown in **Figure 11** (Main, 1980).

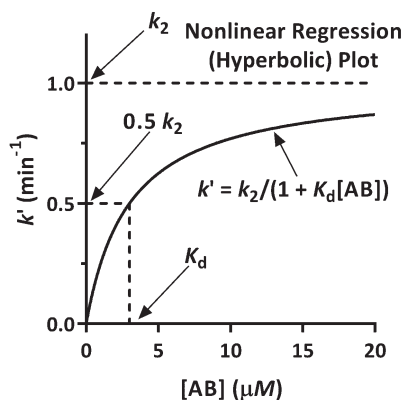


**Figure 11. Hyperbolic plot of  $k'$  vs.  $[AB]$ .** The rectangular hyperbola has an asymptote at  $k' = k_2$ . The  $[AB]$  corresponding to  $0.5 k_2$  is the  $K_d$ . These values and their 95% CI and/or SEM values are easily obtained via nonlinear regression (Ritchie and Prvan, 1996).

The preferred method for determining  $k_2$  and  $K_d$  from kinetic data is nonlinear regression of **Eq. 8**, which yields the best estimates and lowest errors for these constants along with their 95% CI and/or SEM values (Ritchie and Prvan, 1996). Nonlinear regression methods have been readily available for some time, and such methods specifically tailored for Michaelis-Menten and related kinetics are

included in widely used software packages for scientific data analysis and graphing such as GraphPad Prism (current version 8.0; GraphPad Software, La Jolla, CA) and OriginPro (current version 2019; OriginLab, Northampton, MA). Nevertheless, various linear transformations remain popular for categorizing mechanisms of inhibition and determining kinetic constants.

## Linear Transformations

Decades ago, before personal computers and convenient software packages were generally available, **Eq. 8** was rearranged in various ways to linearize the equation, making it easier to obtain values for  $k_2$  and  $K_d$  using graphical methods and/or linear regression. These equations and their corresponding linear plots are referred to by their names from Michaelis-Menten kinetics (Ritchie and Prvan, 1996; Wilkinson, 1961).

Accordingly, **Eq. 9** and its associated plot (**Figure 12**) constitute the Lineweaver-Burk (double-reciprocal) equation and plot:

$$1/k' = (k_2/[AB]K_d) + (1/k_2) \quad (\text{Eq. 9})$$

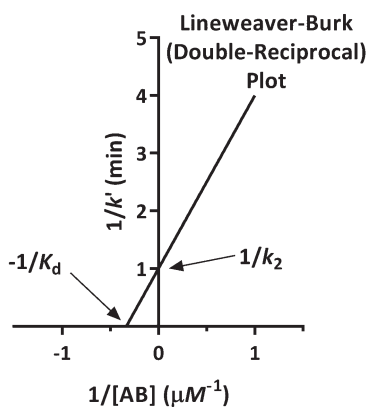


**Figure 12. Lineweaver-Burk (double-reciprocal) plot.** A plot of  $1/k'$  vs.  $1/[AB]$  is a straight line with y-intercept =  $1/k_2$  and x-intercept =  $-1/K_d$  from which  $k_2$  and  $K_d$  can be calculated. However, this linearized form of **Eq. 8** magnifies errors and is undefined for zero values of  $k'$  and  $[AB]$ ; consequently, nonlinear regression of **Eq. 8** should be used to determine  $k_2$  and  $K_d$  (Ritchie and Prvan, 1996; Wilkinson, 1961).

The Lineweaver-Burk (double-reciprocal) plot (**Figure 12**) has enjoyed enormous popularity since its inception, but it greatly magnifies errors, even when values obtained for  $R$  or  $R$ -squared indicate an excellent linear fit to the reciprocally transformed data (Ritchie and Prvan, 1996; Wilkinson, 1961). Indeed, the GraphPad Prism *Curve Fitting Guide* specifically warns users to use a Lineweaver-Burk plot

only for displaying transformed data and not for determining rate and equilibrium constants – it recommends using nonlinear regression instead (GraphPad, 2018c,d).

**Eq. 10** and its graphical representation (**Figure 13**) are the Hanes-Woolf equation and plot:

$$[AB]/k' = [AB]/k_2 + K_d/k_2 \quad (\text{Eq. 10})$$

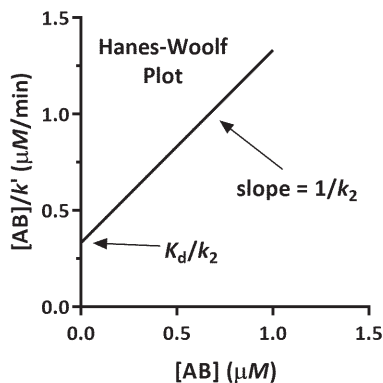


**Figure 13. Hanes-Woolf plot.** A plot of  $[AB]/k'$  vs.  $[AB]$  is a straight line with y-intercept =  $K_d/k_2$  and slope =  $1/k_2$  from which  $k_2$  and  $K_d$  can be calculated. This linearized version of **Eq. 8** can yield better results than the Lineweaver-Burk (double-reciprocal) method (**Figure 12**) (Wilkinson, 1961) but it is still inferior to carrying out nonlinear regression on **Eq. 8** (Ritchie and Prvan, 1996).

The Hanes-Woolf plot (**Figure 13**) is an improvement over the Lineweaver-Burk (double-reciprocal) plot (**Figure 12**) (Wilkinson, 1961) but it is also undefined for zero values of  $k'$ , and because it contains  $[AB]$  on both sides of the equation (**Eq. 10**), it violates the principle of independent variables, so that linear regression is not applicable (Ritchie and Prvan, 1996).

Of the three methods for linearizing equations of the Michaelis-Menten type, e.g., **Eq. 8**, the most problematic is the Eadie-Hofstee approach (**Eq. 11** and **Figure 14**). The main issue is that it contains  $k'$  on both sides of the equation, thus violating the principle of independent variables and rendering linear regression methods invalid (Ritchie and Prvan, 1996).

Overall, despite their stubbornly persistent popularity, linearization approaches for determining  $k_2$  and  $K_d$  from **Eq. 8** are now considered outmoded and prone to magnification of errors. Nonlinear regression of **Eq. 8** is the preferred method (GraphPad, 2018c,d; Ochs, 2010; Ritchie and Prvan, 1996; Wilkinson, 1961; Zierler, 1977).

$$k' = -K_d k' / [AB] + k_2 \quad (\text{Eq. 11})$$



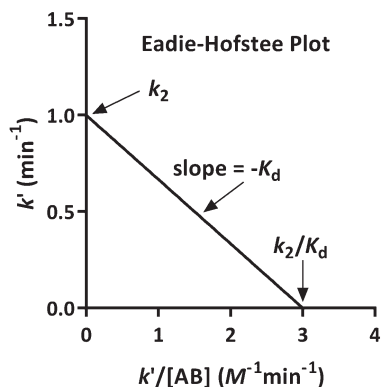


**Figure 14. Eadie-Hofstee plot.** A plot of  $k'$  vs.  $k'/[AB]$  is a straight line with y-intercept =  $k_2$ , slope =  $-K_d$ , and x-intercept =  $k_2/K_d$ , from which  $k_2$  and  $K_d$  can be calculated. This method suffers from the fact that  $k'$  appears on both sides of the equation; therefore,  $k'/[AB]$  is not an independent variable and linear regression is not valid (Ritchie and Prvan, 1996).

### Determining $K_d$ and $k_2$ in the Presence of Substrate

In the case of highly potent OP inhibitors of AChE, in order to satisfy the condition that  $[AB] > 10[E]$  and when  $[AB]$  is not much smaller than  $K_d$ , the reaction rates can be too fast to measure with the standard techniques outlined thus far, whereby the preincubation of the OP inhibitor with AChE is carried out in the absence of substrate. In order to get measurable rates, if  $[AB]$  is decreased so that  $[AB] \ll K_d$ , then **Eq. 8** reduces to pseudo-first-order conditions, where  $k' = k_i[AB]$ . The  $k_2$  and  $K_d$  terms no longer appear in the equation, making it impossible to determine these constants. In such cases, the preincubation can be carried out in the presence of substrate, so that the rate of inhibition will be slowed owing to competition between the substrate and inhibitor. **Eq. 8** can then be modified to include a term for the competitive influence of the substrate:

$$k' = k_2 / \{1 + (K_d/[AB])[1 + ([S]/K_m)]\} \tag{Eq. 12}$$

Where  $[S]$  = substrate concentration and  $K_m$  = the Michaelis constant for the substrate (Aldridge and Reiner, 1972; Kemp and Wallace, 1990; Main, 1980; O'Brien, 1968). With known values for  $[S]$  and  $K_m$ , the unknowns  $k_2$  and  $K_d$  can be determined via nonlinear regression of **Eq. 12**. Alternatively,  $k_i$  can be determined on its own using pseudo-first-order conditions as described by **Eq. 3-4** and **Figure 9**.

### Literature PDP Values for Paraoxon Inhibition of Rat and Human AChE

When comparing rate and equilibrium constants between enzyme sources (e.g., tissue and species), it is important to keep all other conditions and computational methods as correct and equivalent as possible and to ensure that the biochemical principles applying to the determinations have been

observed. When such criteria are met,  $k_i$ ,  $k_2$ , and  $K_d$  values represent PDPs of inhibition by a given OP compound and source of AChE.

**Table 1. Inhibition Constants for Paraoxon against Human and Rat AChE<sup>a</sup>**

Species	Tissue	pH	Buffer <sup>b</sup> (mM)	T (°C)	Method <sup>c</sup>	$K_d$ ( $\mu$ M)	$k_2$ (min <sup>-1</sup> )	$k_i$ ( $\mu$ M <sup>-1</sup> min <sup>-1</sup> )	Ref <sup>d</sup>
Human	Recombinant	7.4	Phos 50	25	DR	---	---	0.7±0.3	(1)
Human	Recombinant	8.0	Phos 50	27	DR	0.98±0.02	1.0±0.01	1.0±0.01	(2)
Human	Recombinant	8.0	Phos 50	27	PFO	---	---	0.97±0.02	(2)
Human	Brain <sup>e</sup>	7.4	Phos 100	37	NLR	---	0.26±0.056	---	(3)
Human	RBC	7.4	Phos 100	37	NLR	---	0.30±0.022	---	(3)
Human	RBC	7.4 <sup>f</sup>	Tris 50	37	DR	0.73±0.10	0.64±0.12	0.86±0.11	(4)
Human	RBC	7.4	Phos 100	37	PFO	---	---	3.3±0.05	(5)
Human	RBC	7.4	MOPS 100	37	PFO	---	---	2.2±0.04	(5)
Human	RBC	7.4	Tris 100	37	PFO	---	---	1.8±0.09	(5)
Human	RBC	7.4	Tyrode	37	PFO	---	---	3.1±0.08	(5)
Human	RBC	7.4	Phos 100	37	NLR	0.9±0.024	3.1±0.063	3.3±0.25	(6)
Rat	RBC	7.4	Phos 100	37	NLR	0.7±0.024	1.1±0.097	1.5±0.063	(6)
Rat	Brain 5k x g <sup>h</sup>	7.4 <sup>f</sup>	Tris 50	30	DR	1.3±0.24	0.35±0.064	0.40±0.020	(7)
Rat	Brain 5k x g <sup>h</sup>	7.4 <sup>f</sup>	Tris 50	37	DR	0.49±0.012	0.40±0.027	0.86±0.033	(7)
Rat	Brain Homog <sup>g</sup>	7.4 <sup>f</sup>	Tris 50	37	DR	2.0 ±0.31	2.3±0.12	1.2±0.11	(4)
Rat	Brain Homog <sup>g</sup>	8.0	Phos 100	37	DR	14±7.7	19±6.7	1.4±0.19	(8)
Rat	Brain 100k x g <sup>i</sup>	8.0	Phos 100 <sup>j</sup>	37	DR+S	1.6±0.67	2.1±0.60	1.5±0.02	(9)
Rat	Brain Slices	7.6	Tris	25	DR	0.072	0.03	0.43	(10)
Rat	Brain Homog <sup>g</sup>	7.4	Phos 100	RT	DR	---	---	0.36	(11)
Rat	Brain Homog <sup>k</sup>	8.0	Phos 100	25	DR+S	1.51±0.29	4.720±0.30	3.23±0.15	(12)

<sup>a</sup> Data for  $K_d$ ,  $k_2$ , and  $k_i$  are mean ± SEM rounded to two significant figures not including placeholder zeros. Note that whereas  $k_i = k_2/K_d$  for corresponding individual determinations, calculating mean  $k_i$  values would require using the harmonic mean rather than the arithmetic mean for  $K_d$ .

<sup>b</sup> Buffers: MOPS = 3-[N-morpholino]propanesulfonic acid; Phos = NaPhosphate; Tris = Tris[hydroxymethyl]amino-methane; Tyrode = 125 mM NaCl, 24 mM NaHCO<sub>3</sub>, 5.4 mM KCl, 1 mM MgCl<sub>2</sub>, 1.8 mM CaCl<sub>2</sub>, 10 mM glucose, pH 7.4 at 37 °C, aerated with 95% O<sub>2</sub>/5% CO<sub>2</sub> (v/v), and cuvettes sealed during assay.

<sup>c</sup> Mathematical method: DR = double-reciprocal; DR+S = double-reciprocal in presence of substrate; NLR = non-linear regression; PFO = pseudo-first-order.

<sup>d</sup> References: (1) Amatai et al., 1988; (2) Ordentlich et al., 1996; (3) Herkert et al., 2012; (4) Coban et al., 2016; (5) Wille et al., 2011; (6) Worek et al., 2008; (7) Carr and Chambers, 1996; (8) Cohen et al., 1985; (9) Kemp and Wallace, 1990; (10) Kiffer and Delamanche, 1983; (11) Worek et al., 2011; (12) Milatovic and Dettbarn (1996).

<sup>e</sup> Human glioblastoma tissue.

<sup>f</sup> pH values were calibrated at pH 7.4 in Tris buffer at 25 °C; however, with a temperature coefficient of -0.026 pH unit per °C, the actual pH would be 7.3 at 30 °C and 7.1 at 37 °C (Durst and Staples, 1972).

<sup>g</sup> Brain homogenate.

<sup>h</sup> 5000 x g pellet from brain homogenate.

<sup>i</sup> 100,000 x g pellet.

<sup>j</sup> 100 mM NaPhosphate buffer pH 8.0 containing 3 mM NaEDTA, 0.5% (w/v) Triton X-100, and 400 mM NaCl.

<sup>k</sup> Brain homogenate in 100 mM phosphate buffer pH 8.0 containing 0.5% (w/v) Triton X-100.

Literature values for  $k_2$ ,  $K_d$ , and/or  $k_i$  are presented in **Table 1** for the relatively potent AChE inhibitor, paraoxon (the active metabolite of the OP insecticide, parathion) against rat and human AChE. The table includes information on species, tissue, buffer, temperature, mathematical method, and PDP for each of the 12 references. For ease of comparison, the inhibition constants have been converted as needed into consistent units. Even so, comparisons are difficult because of differences in tissue, tissue preparation, pH, buffer, temperature, and computational method. Nevertheless, taking the inhibition constants at face value, these have been plotted in **Figure 15**; however, because the  $K_d$  and  $k_2$  data from references (8) and (10) were statistical outliers several standard deviations away from the mean, the  $K_d$ ,  $k_2$  and  $k_i$  data from these studies were omitted from **Figure 15**.

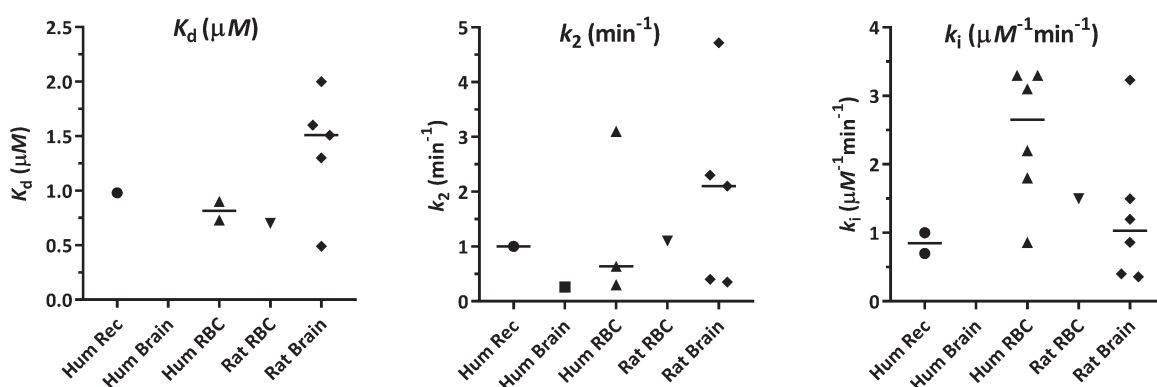


**Figure 15.** Literature values of inhibition constants for paraoxon inhibition of AChE. Data from **Table 1**, except values from references (8) and (10) were omitted as statistical outliers. Panels from left to right show data for  $K_d$ ,  $k_2$ , and  $k_i$ , respectively. Within each panel, the AChE sources from left to right are human recombinant, human brain (glioblastoma), rat RBC, and rat brain. Each point represents an individual mean value from **Table 1**. The horizontal bar in each column marks the median value for that group.

Inspection of **Table 1** and **Figure 15** reveals a number of methodological issues and data gaps listed below. Recognizing the shortcomings of previous investigations will be helpful in designing future studies with the goal of correctly carrying out determinations of PDP for OP-compound inhibition of AChE and minimizing variability so that meaningful comparisons of human and rat enzyme can be made.

*Tissue source within human and rat.* Subsequent sections of this paper will show that the catalytic domain of AChE is encoded by a single gene within a given species so that the enzyme is the same in all tissue sites (Massoulié, 2002). Molecular polymorphisms occur only in the C-terminal region that is involved in membrane anchoring (Liang et al., 2009). For practical reasons, a plasma membrane preparation of RBC AChE (RBC “ghosts”) is recommended for each species (human and rat) (Dodge et al., 1963). **Table 1** has seven entries for human RBC AChE but only a single entry for rat RBC AChE.

Moreover, only two entries for human RBC AChE included determinations for all three inhibition constants; these measurements were carried out in different buffers and the results analyzed using different mathematical methods.

*Assay method.* Not explicitly shown in **Table 1** are the AChE assay methods. Most studies used the classical Ellman spectrophotometric assay with acetylthiocholine (ATCh) as the substrate (Ellman et al., 1961). This method is widely accepted and recommended for future studies. Activity can be expressed in various ways, but it is often normalized as specific activity according to protein content, e.g., nmol product formed per minute per mg protein. Protein can be quantified in various ways, including colorimetrically using the classic Lowry method with bovine serum albumin at the standard (Lowry et al., 1951).

*Buffer and pH.* Various pH values (7.4, 7.6, 8.0) and buffers (50 or 100 mM phosphate with or without added salts and/or detergent; Tyrode's solution; MOPS; and 50 or 100 mM Tris). Use of Tris is not recommended because of its negative temperature coefficient. For example, if 50 mM Tris were calibrated to pH 7.4 at 25 °C, the actual pH at 37 °C would be 7.1 (Durst and Staples, 1972). In addition, Tris is known to be a competitive inhibitor of AChE (Pavlic, 1967; Wille et al., 2011). The recommended buffer is 50-100 mM Na phosphate at the presumptive physiological pH of 7.4. Optionally, 0.2 -1.0% (w/v) Triton X-100 could be added to solubilize AChE (Spinedi et al., 1989; 1993).

*Solvent for OP stock solutions.* Not explicitly stated in **Table 1** are the organic solvents used for preparing OP stock solutions. Various water-miscible solvents have been employed in such studies, including acetone, acetonitrile, DMF, DMSO, ethanol, and isopropanol. Any of these solvents could be used as long as the OP compounds are sufficiently soluble to achieve the necessary test concentrations. To avoid hydrolysis of the OP compounds, the solvents should be anhydrous. If alcohols different from the O-alkyl groups attached to the phosphorus atom are used, the compounds should be checked for possible transesterification.

*Temperature.* Studies were carried out at RT, 25, 27, 30, or 37 °C. The recommended temperature is 37 °C, which is the normal mean physiological body temperature for humans (Karakitsos and Karabinis, 2008), and normal rat body temperature is reportedly close to this value (Sharp and Villano, 2012).

*Computational method.* Eight of the 12 reported studies used the double reciprocal technique. Only two studies used the preferred nonlinear regression method (GraphPad, 2017b; Hofstee, 1959; Martin, 1997; Ochs, 2010; Ritchie and Prvan, 1996; Wilkinson, 1961; Zierler, 1977), and both of these studies were from the same laboratory.

When the  $K_d$  and  $k_2$  components of  $k_i$  are sought, the recommended method is nonlinear regression of Eq. 8 above (GraphPad, 2017c). Nonlinear regression will yield not only  $K_a$  and  $k_2$ , but also the associated 95% confidence intervals, standard errors, and goodness of fit.

The standard errors reported from the studies using the double-reciprocal method are incorrect – the authors used values from several determinations to calculate mean and SE values in the usual manner, which would be expected to yield artificially low errors within a given study. Nevertheless, **Table 1** and **Figure 15** show considerable variation across studies for rat brain  $K_d$ ,  $k_2$ , and  $k_i$  as well as human RBC  $k_i$ . However, for a given inhibition constant, values for rat and human overlapped. Future studies using appropriate and consistent biochemical and mathematical methods would be expected to yield improved accuracy and precision.

When only the  $k_i$  is needed, pseudo-first-order conditions may be used to generate primary kinetic plots and secondary plots from which the  $k_i$  can be calculated, as shown above in **Eq. 3-4** and **Figure 9** (Kropp and Richardson, 2003). Indeed, the  $k_i$  is a suitable measure of overall inhibitory potency that could be used for comparisons across compounds and species when it is not feasible to obtain accurate determinations of the affinity ( $K_d$ ) and phosphorylation rate ( $k_2$ ) components.

As detailed in the following sections, interspecies variation in the numerical values of  $k_i$ ,  $k_2$ , and  $K_a$  are expected to decrease with increasing structural homology of the enzyme, and intraspecies variation in these values are expected to be sufficiently small to lack biological significance.

## Molecular Forms and Tissue Distribution of AChE

This section reviews the different molecular forms of AChE across different tissues. AChE in mammals, including humans and rats, is encoded by a single gene in each species (Massoulié *et al.*, 2008; Taylor *et al.*, 1993). Nevertheless, owing to alternative RNA splicing, different polymorphic forms are expressed in various tissues, including brain, erythrocytes (RBCs), and skeletal muscle. However, the catalytic domains of these molecular forms within each species are identical (**Figure 16**).

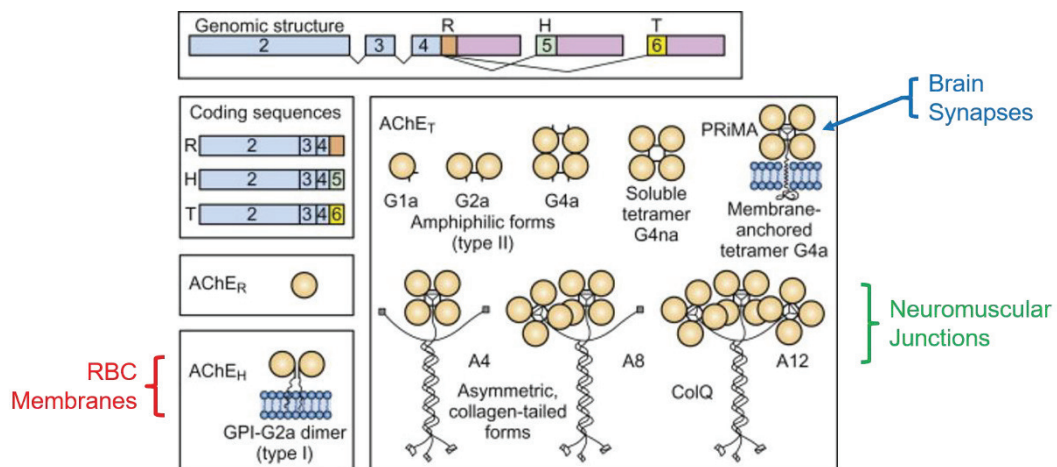


**Figure 16.** AChE molecular forms. The mammalian AChE gene comprises three exons giving rise to molecular forms found in various tissues. The catalytic subunits (yellow spheres) encoded by exons 2, 3, and 4 are identical in each molecular form. Exon 1 codes for the N-terminal signal sequence that is cleaved from the finished catalytic subunit. Alternative splice sites in exons 4, 5, and 6 give rise to the coding sequences for three molecular forms of AChE: R (readthrough), H (hydrophobic), and T (tail). These three molecular forms have identical catalytic subunits and differ only in their C-terminal regions. AChE<sub>R</sub> is a minor form normally expressed at low levels. AChE<sub>H</sub> is found on erythrocyte (red blood cell, RBC) plasma membranes. AChE<sub>T</sub> is found in brain and spinal cord as soluble (globular, G) monomers, dimers, or tetramers or bound to synaptic membranes by association with a proline-rich membrane anchor (PRiMA). AChE<sub>T</sub> is also found in nerve-muscle synapses (neuromuscular junctions) with one, two, or three tetramers attached to a collagen tail (ColQ) that is anchored to the extracellular matrix surrounding the postsynaptic muscle membrane. These tetramer-ColQ assemblies are dubbed A4, A8, and A12 to denote the overall asymmetry and the number of catalytic subunits. (Adapted from Fisher and Wonnacott, 2012)

Referring to **Figure 16**, the genomic structure of AChE includes six exons. Exon 1 encodes a signal sequence that is cleaved from the final AChE product. The catalytic domain of AChE is encoded by Exons 2, 3, and 4, and is identical in all molecular forms of AChE within a given species. Splice sites in exons 4, 5, and 6 generate three main forms of coding sequences for three forms of AChE that differ only in their C-terminal regions. These forms are known as R (readthrough), H (hydrophobic), and T (tail) (Massoulié *et al.*, 2002).

The R-form of AChE is normally found only in small amounts in various tissues. Its function is unclear, but relatively recent work indicates that its expression is increased in Alzheimer's disease, and it may play an anti-apoptotic role following certain forms of cellular stress (Campanari et al., 2016; Zimmermann, 2013).

The H-form exists as dimers attached to plasma membranes of erythrocytes (RBCs) following posttranslational modification of the C-terminal region by glycerophosphatidylinositol (GPI). The function of AChE in RBCs is unclear, although it is known to be the YT blood group antigen (Bartels et al., 1993).

In nerve-muscle synapses (neuromuscular junctions), the T-form of AChE is tethered to the extracellular matrix of muscle by a collagen protein, ColQ, which can accommodate one, two, or three tetrameric AChE units; these forms are named A4, A8, and A12 to denote their overall asymmetry and the number of catalytic subunits. Elsewhere in the CNS and PNS, the T-form of AChE is found as soluble (globular, G) monomers, dimers, or tetramers, and predominantly in synapses as tetramers attached to membranes by association of the C-terminus region of the enzyme with a proline-rich membrane anchor (PRiMA) protein (Fisher and Wonnacott, 2012).

## Intraspecies Sequence Homology of Brain and RBC AChE within Human or Rat

---

The protein sequence alignment of human brain and RBC AChE is shown in **Figure 17**. The sequences of the N-terminal signal peptide and catalytic domain are identical. As expected, the sequences of the C-terminal anchor region differ; this is in keeping with the different modes of tethering AChE to RBC or synaptic membranes. The catalytic triad residues (Ser234, Glu365, His478) of the active site appear distant from each other in the linear sequence, but they are in close proximity in the properly folded three-dimensional protein (Uniprot, 2017a).

Similarly, **Figure 18** displays the protein sequence alignment of rat brain and RBC AChE. As is the case with the human enzyme, the rat sequences for the N-terminal signal peptide and catalytic domain are identical. Here again, the C-terminal anchor regions differ, as expected for different means of attachment of the enzyme to RBC or synaptic membranes. The same sequence numbering scheme is used here for human and rat; therefore, the active site residues are found at Ser234, Glu365, and His478 in the rat brain and RBC enzymes (Uniprot, 2017b).

**Figures 17 and 18** illustrate the fact that the catalytic domains of brain and RBC AChE are identical within a given species, i.e., human or rat. Consequently, their responses to inhibitors are highly similar (Herkert *et al.*, 2012), and inhibition of RBC AChE has been used as a surrogate for brain AChE inhibition as well as a biomarker of exposure to OP insecticides (Carlock *et al.*, 1999; Chen *et al.*, 1999). Therefore, human and rat RBCs are the recommended sources of AChE for the proposed studies to determine pharmacodynamic parameters for AChE inhibition by OP compounds.

AChE activity can be assayed in suspensions of RBC plasma membranes (RBC “ghosts”) or in solutions of RBC AChE solubilized with phosphatidylinositol phospholipase C (PIPLC) or detergents, such as Triton-X 100. However, PIPLC quantitatively releases AChE from rat RBCs, but only partially from human RBCs (Barton *et al.*, 1985). Literature concerning effects of membrane composition or fluidity on AChE activity is somewhat equivocal, but on balance, it appears that Arrhenius plots of membrane-bound and solubilized AChE are identical, indicating minimal influence of the membrane environment on AChE activity (Barton *et al.*, 1985; Spinedi *et al.*, 1993).



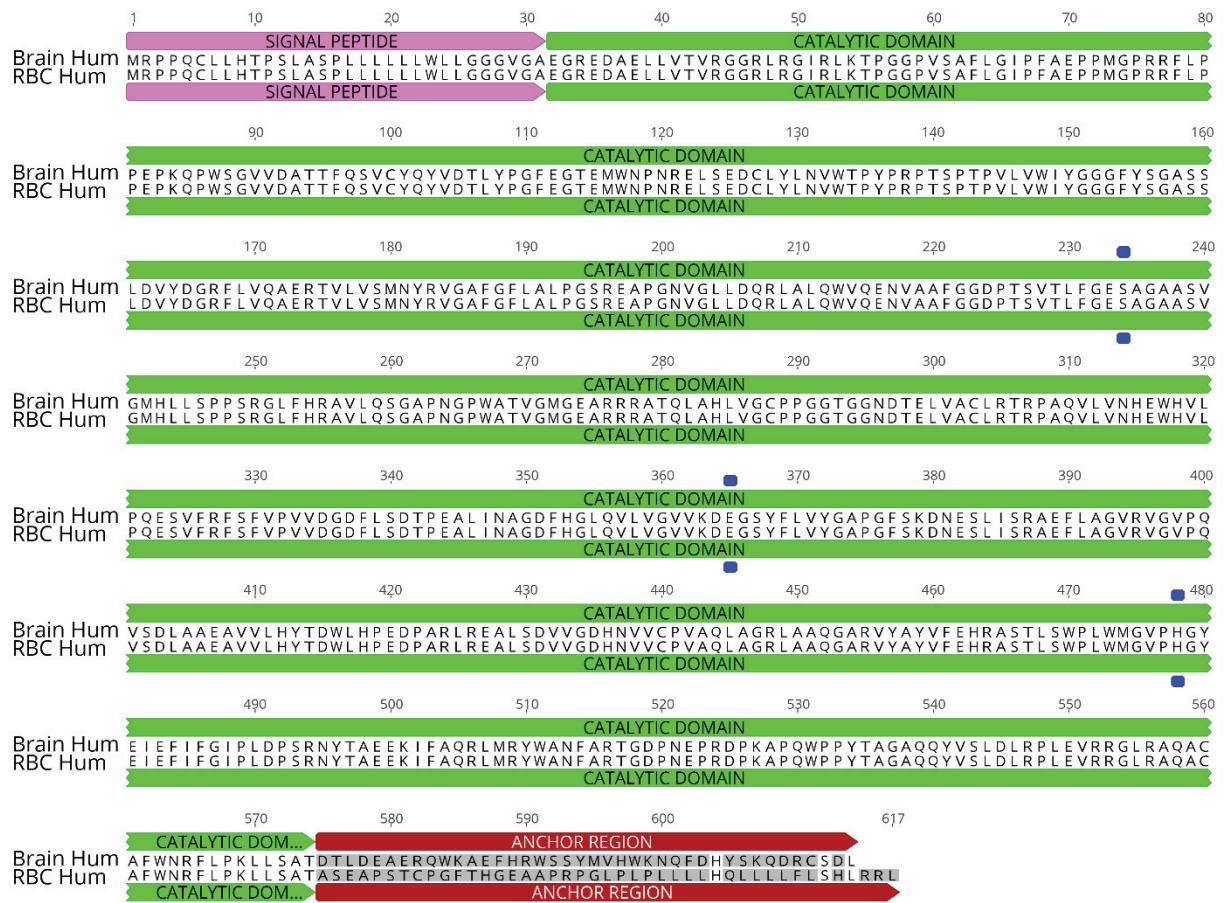


**Figure 17.** Sequence alignment of human brain and human RBC AChE. N-terminal signal peptide = magenta. Catalytic domain = green. Catalytic triad residues (Ser234, Glu365, His478) in active site = blue. C-terminal anchor region = dark red. Identical residues = unshaded. Non-identical residues = gray-shaded. Sequence identity in catalytic domain = 100% (Uniprot, 2017a). Alignment and annotations carried out with Geneious 10.2.2 (Geneious, 2017) using the default Geneious algorithm and identity matrix.

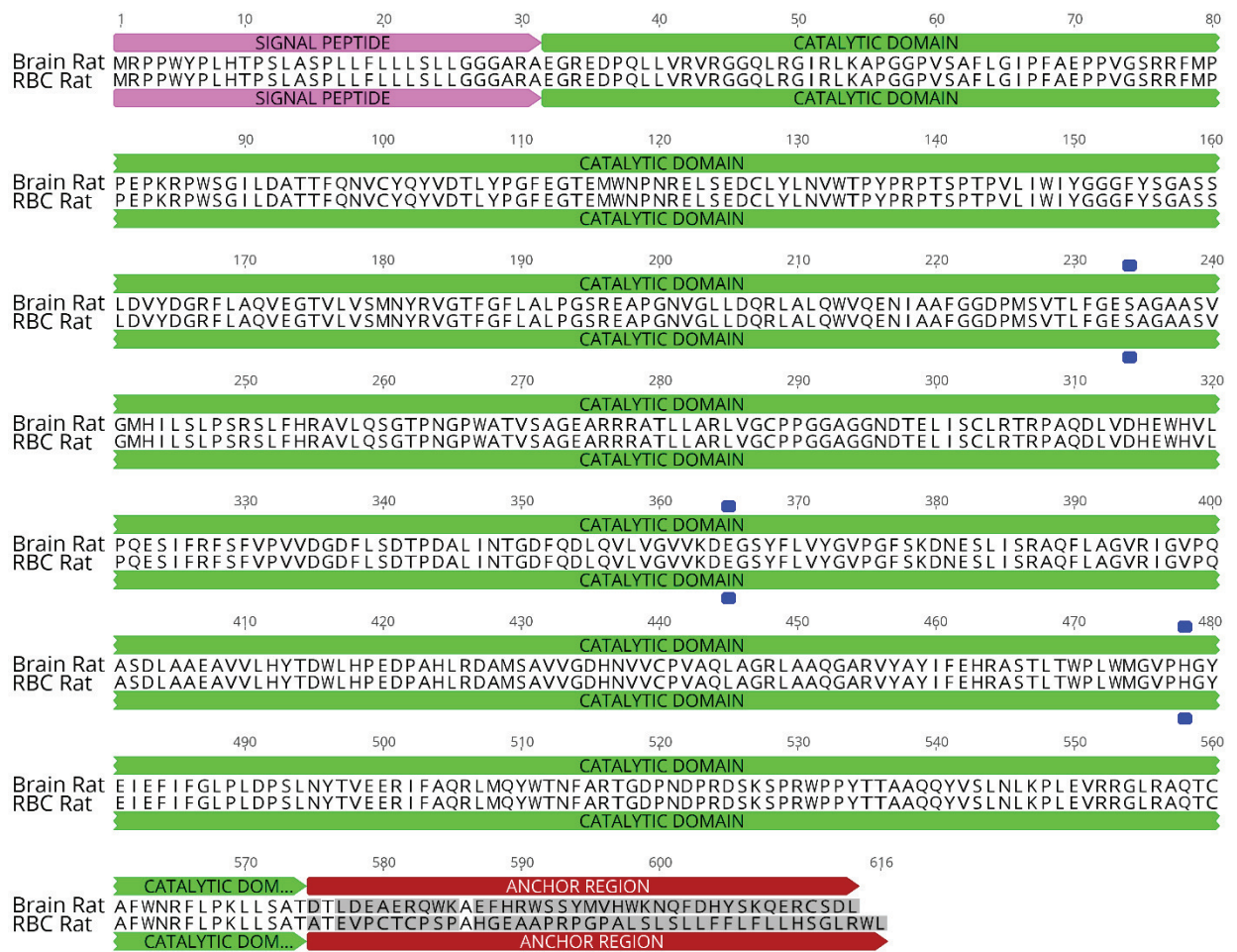


**Figure 18.** Sequence alignment of rat brain and rat RBC AChE. N-terminal signal peptide = magenta. Catalytic domain = green. Catalytic triad residues (Ser234, Glu365, His478) in active site = blue. C-terminal anchor region = dark red. Identical residues = unshaded. Non-identical residues = gray-shaded. Sequence identity in catalytic domain = 100% (Uniprot, 2017b). Alignment and annotations carried out with Geneious 10.2.2 (Geneious, 2017) using the default Geneious algorithm and identity matrix.

## Interspecies Sequence Homology of Human and Rat AChE for Brain or RBC

---

**Figure 19** shows the protein sequence alignment for human and rat brain AChE. The gray-shaded residues mark sites that are different between the two sequences. The sequence identity of the catalytic domains is 88.6% (sequence similarity is 94.1%), and the active site residues coincide (Uniprot, 2017a,b).

The protein sequence alignment for human and rat RBC AChE is shown in **Figure 20**. The sequence identity between the catalytic domains is 88.6% (sequence similarity is 94.1%), and the active site residues Ser234, Glu365, and His478 are in alignment (Uniprot, 2017a,b).

Thus, the catalytic domains of human and rat AChE are not identical, but they are highly homologous. The high sequence homology is an important factor leading to the working hypothesis, which will be tested by carrying out the proposed study.

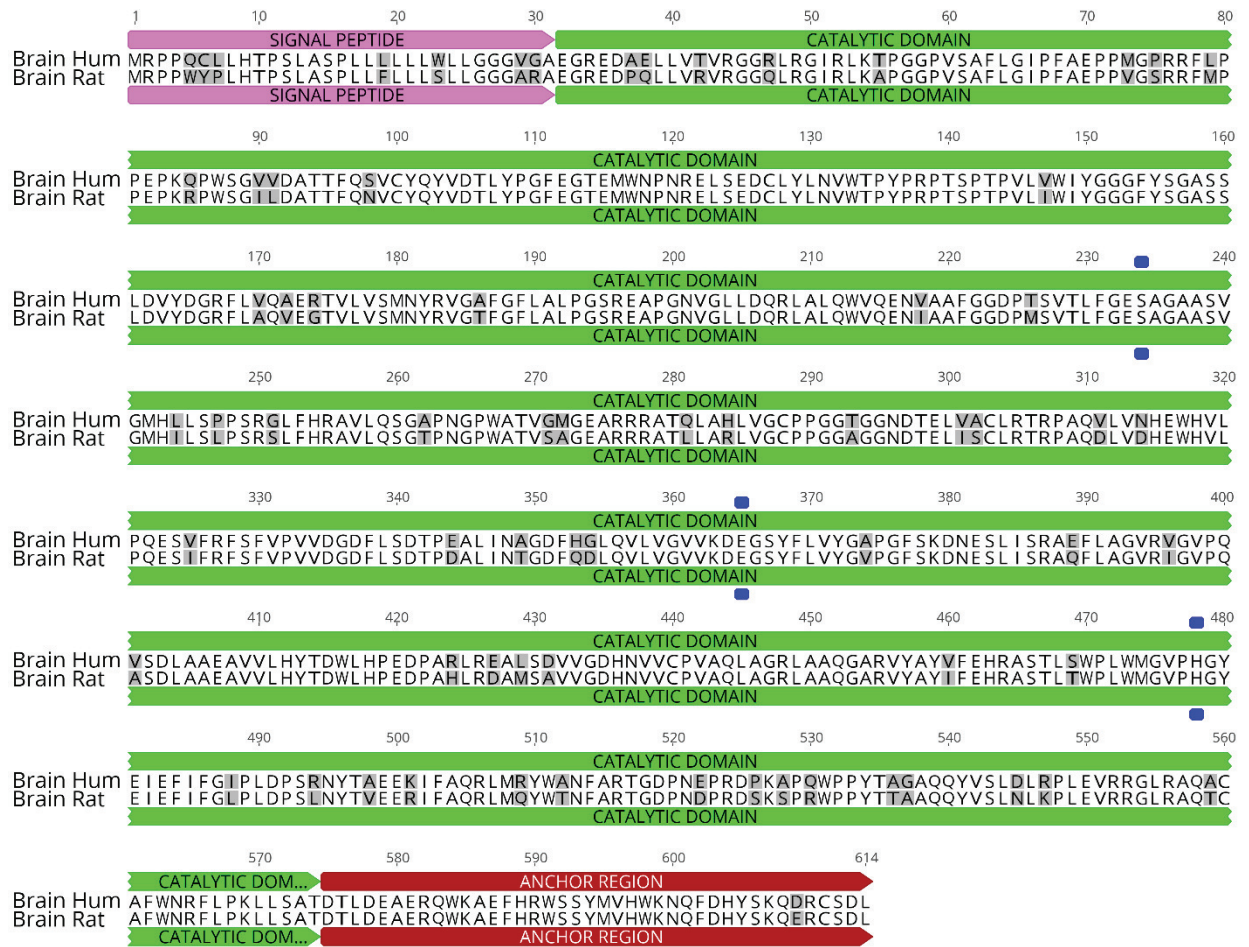


**Figure 19.** Sequence alignment of human brain and rat brain AChE. N-terminal signal peptide = magenta. Catalytic domain = green. Catalytic triad residues (Ser234, Glu365, His478) in active site = blue. C-terminal anchor region = dark red. Identical residues = unshaded. Non-identical residues = gray-shaded. Sequence identity in catalytic domain = 88.6% (sequence similarity = 94.1%) (Uniprot, 2017a,b). Alignment and annotations carried out with Geneious 10.2.2 (Geneious, 2017) using the default Geneious algorithm and identity matrix.

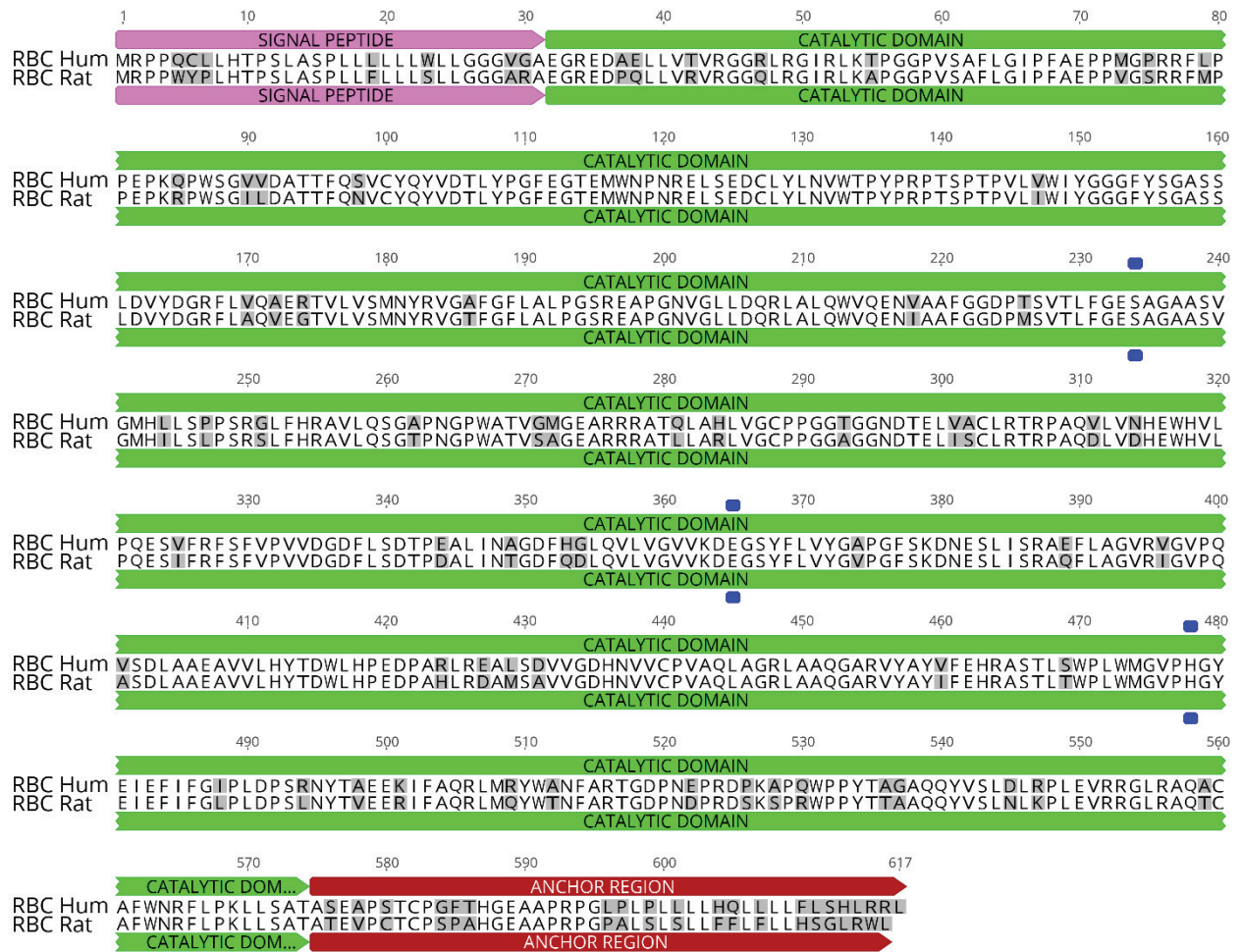


**Figure 20.** Sequence alignment of human RBC and rat RBC AChE. N-terminal signal peptide = magenta. Catalytic domain = green. Catalytic triad residues (Ser234, Glu365, His478) in active site = blue. C-terminal anchor region = dark red. Identical residues = unshaded. Non-identical residues = gray-shaded. Sequence identity in catalytic domain = 88.6% (sequence similarity = 94.1%) (Uniprot, 2017a,b). Alignment and annotations carried out with Geneious 10.2.2 (Geneious, 2017) using the default Geneious algorithm and identity matrix.

## Three-dimensional (3D) Structural Homology of Human and Rat AChE

---

The 3D structure of human AChE in complex with unaged sarin was taken from the Protein Data Bank (PDB) X-ray crystal structure PDB ID = 5FPQ (PDB, 2017a). Using the software suite YASARA-Structure 17.4.17, missing loops were repaired and optimized, the structure was energy-minimized in explicit solvent, the sarin ligand was removed, and the overall hydrogen-bonding network was optimized (YASARA, 2017). The resulting structure is shown in **Figure 21**.

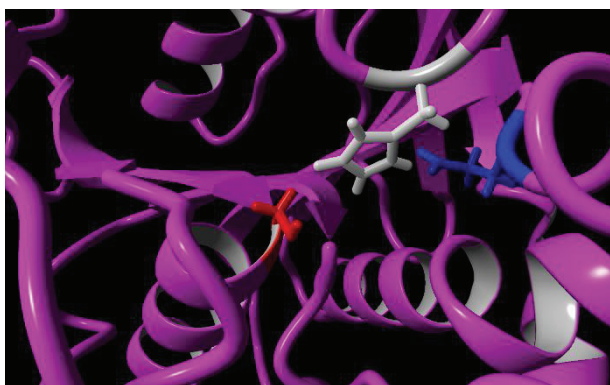


**Figure 21.** 3D structure of human AChE. Ribbon view (magenta). Catalytic triad residues (stick view): Ser234 = red; His478 = gray; Glu365 = blue (PDB ID = 5FPQ; refined and rendered by YASARA-Structure 17.4.17). (YASARA, 2017)

There are no 3D structures available for rat AChE. However, there are many X-ray crystal structures in the PDB for mouse AChE, which has 98.2% sequence identity with rat AChE (Uniprot, 2017c). Therefore, it is possible to construct a 3D homology model for rat AChE from the mouse structure by carrying out threading, homology modeling, or *in silico* mutagenesis (Dorn et al., 2014). Here, the latter approach was chosen and carried out with YASARA-Structure 17.4.17, using PDB ID = 2Y2V – mouse AChE in complex with unaged sarin (PDB, 2017b). After performing the *in silico* mutagenesis, using YASARA-Structure 17.4.17, missing loops were repaired and optimized, the structure was energy-minimized in explicit solvent, the sarin ligand was removed, and the overall hydrogen-bonding network was optimized (YASARA, 2017). The resulting structure is shown in **Figure 22**.

**Figure 23** shows the 3D alignment of the human X-ray crystal structure and the rat homology model of AChE. The structures are nearly congruent, with an overall root mean square deviation (RMSD) of 0.811 Å, which reflects excellent agreement between the two structures. For example, the majority of pairs of X-ray crystal structures of the same protein in the PDB have RMSD values < 1.2 Å and pairs of homology models of the same protein can have average RMSD values as high as 4.5 Å, depending upon the degree of homology (Kufareva and Abagyan, 2012). Moreover, each of the residues of the catalytic

triad is almost exactly superimposed. This result supports the hypothesis that human and rat AChE would be expected to interact similarly with OP inhibitors of the enzyme.

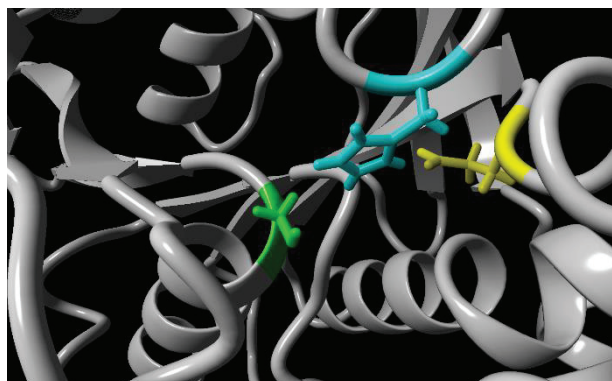


**Figure 22.** 3D structure of rat AChE. Ribbon view (gray). Catalytic triad residues (stick view): Ser234 = green; His478 = cyan; Glu365 = yellow (PDB ID = 2Y2V mouse mutated to rat AChE; refined and rendered by YASARA-Structure 17.4.17) (YASARA, 2017).

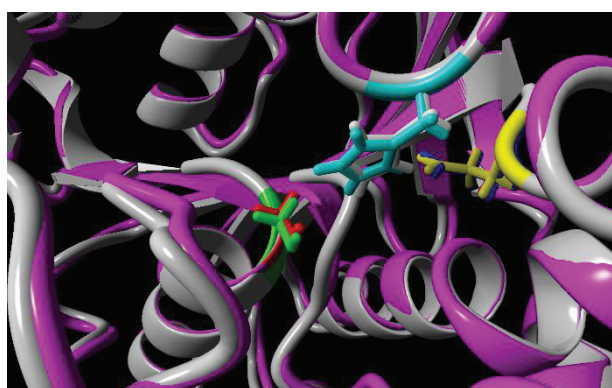


**Figure 23.** 3D alignment of human and rat AChE. Human ribbon view (magenta); rat ribbon view (gray). Human catalytic triad residues (stick view): Ser234 = red; His478 = gray; Glu365 = blue. Rat catalytic triad residues (stick view): Ser234 = green; His478 = cyan; Glu365 = yellow. Overall RMSD = 0.811 Å. Aligned and rendered by YASARA-Structure 17.4.17 using the MUSTANG procedure (Konaguthru et al., 2006; YASARA, 2017)

## Potential Intraspecies Variations in AChE PDPs

---

The PDPs of AChE are determined by the amino acid sequence of the catalytic domain, which in turn dictates the 3D structure of the enzyme. Therefore, variables such as age, gender, pregnancy, or disease status would not be expected to change the amino acid sequence or thereby alter the PDPs of the enzyme, although such variables could influence PK factors. In particular, with respect to age and developmental aspects, there have been no reports of a fetal form of human or rat AChE that differs in sequence from AChE in adults (Uniprot, 2017a,b).

There have been numerous human studies on the relationship between AChE activity (usually in RBCs) and age of the individual (e.g., Arrieta et al., 2009; Garcia-Lopez and Monteoliva, 1988; Ramenjak, 1998) or of RBCs within individuals (e.g., Lefkowitz et al., 2007), with studies variously reporting increases, decreases, or no change. Most of these investigations did not examine changes in intrinsic PDPs of human AChE with age. However, one study did measure the apparent  $K_m$  for ACh in human RBC AChE and found no significant change with age from 34 weeks premature to 32 years adult (Ecobichon and Stephens, 1973).

In a human study of 818 males and 173 females, there were no significant gender differences in AChE activity (Arrieta et al., 2009). In a study involving 117 males and 111 females aged 0 - 72 years with 32 pregnant women aged 20 - 40 years, there were no significant differences in RBC AChE activity by age or gender, but there was a significant increase in RBC AChE activity in pregnant women (Rumenjak, 1998). The increased RBC AChE activity in pregnant women would not be consistent with an increased intrinsic sensitivity to AChE inhibitors for pregnant women.

Studies in rats generally find an inverse correlation between sensitivity to OP insecticide acute toxicity and age. However, this has been attributed to age-related PK factors rather than age-related changes in the intrinsic PDPs of AChE (Giordano and Costa, 2012; Mortensen et al., 1998; Vidair, 2004).

Changes in posttranslational modifications (PTMs) of AChE associated with differences in age, gender, disease status, or genetics could potentially alter its PDPs (Nalivaeva and Turner, 2001). Apart from four stable disulfide bonds (three interchain and one interchain) and one glycerophosphatidylinositol (GPI) attachment site in the RBC anchor domain, there are three known PTM sites in human and rat AChE. All three of these loci are N-glycosylation sites located on the protein surface far from the catalytic center (Uniprot, 2007a,b). Mutating these sites to prevent N-glycosylation had no significant effect on activity or PDPs for ACh hydrolysis (Velan et al., 1993). Furthermore, elimination of the interchain disulfide bond or deletion of the C-terminal anchor domain had no effect on catalytic activity (Liang et al., 2009; Velan et al., 1991).



Genetic mutations within the catalytic domain of AChE would be the only factor with the potential to alter intrinsic PDPs of the enzyme. One naturally occurring human AChE variant has been reported that was expressed *in vitro* and shown to decrease thermal stability and decrease the rate of inhibition by paraoxon (Valle et al., 2011). However, this mutation is extremely rare; indeed, as of 2016, no disease or increased risk of anti-AChE toxicity has been associated with mutations in AChE (Lockridge et al., 2016). The most frequent AChE variant is associated with the YT blood group antigen, and it has normal AChE activity (Masson et al., 1994).

With the foregoing considerations in mind, no significant intraspecies variations in human or rat AChE PDPs are expected.

## References

---

- Aldridge, W.N., and Reiner, E. (1972). *Enzyme Inhibitors as Substrates: Interactions of Esterases with Esters of Organophosphorus and Carbamic acids*. North-Holland, Amsterdam. 328 pp.
- Amatai, G., Moorad, D., Adani, R., and Doctor, B.P. (1998). Inhibition of acetylcholinesterase and butyrylcholinesterase by chlorpyrifos-oxon. *Biochem. Pharmacol.* **56**, 293-299.
- Arrieta, D.E., McCurdy, S.A., Henderson, J.D., Lefkowitz, L.J., Reitstetter, R., and Wilson, B.W. (2009). Normal range of human red blood cell acetylcholinesterase activity. *Drug Chem. Toxicol.* **32**, 182-185.
- Bartels, C.F., Zelinski, T., and Lockridge, O. (1993). Mutation at codon 322 in the human acetylcholinesterase (ACHE) gene accounts for YT blood group polymorphism. *Am. J. Hum. Genet.* **52**, 928-936.
- Barton, P.L., Futerman, A.H., and Silman, I. (1985). Arrhenius plots of acetylcholinesterase activity in mammalian erythrocytes and in *Torpedo* electric organ. *Biochem. J.* **231**, 237-240.
- Basova, N.E., and Rozengart, E.V.J. (2009). Identical reactivity of brain and erythrocyte cholinesterases of some mammals. *J. Evol. Biochem. Biophys.* **45**, 169-176.
- Campanari, M.-L., Navarrete, F., Ginsberg, S.D., Manzanares, J., Saez-Valero, J., and Garcia-Ayllon, M.-S. (2016). Increased expression of readthrough acetylcholinesterase variants in the brains of Alzheimer's disease patients. *J. Alzheimers Dis.* **53**, 831-841.
- Carlock, L.L., Chen, W.L., Gordon, E.G., Kileen, J.C., Manley, A., Meyer, L.S., Mullin, L.S., Pendino, K.J., Percy, A., Sargent, D.E., Seaman, L.R., Svanborg, N.K., Stanton, R.H., Tellone, C.I., and Van Goethem, D.L. (1999). Regulating and assessing risks of cholinesterase-inhibiting pesticides: divergent approaches and interpretations. *J. Toxicol. Environ. Health B Crit. Rev.* **2**, 105-160.
- Carr, P.D., and Ollis, D.L. (2009). Alpha/beta hydrolase fold: an update. *Protein Pept. Lett.* **16**, 1137-1148.
- Carr, R.L., and Chambers, J.E., (1996). Kinetic analysis of the in vitro inhibition, aging, and reactivation of brain acetylcholinesterase from rat and channel catfish by paraoxon and chlorpyrifos-oxon. *Toxicol. Appl. Pharmacol.* **139**, 365-373.
- Case, D. (1994). Toxicokinetics: some definitions. *Drug Inf. J.* **28**, 145-149.
- Chen, W.L., Sheets, J.J., Nolan, R.J., and Mattsson, J.L. (1999). Human red blood cell acetylcholinesterase inhibition as the appropriate and conservative surrogate endpoint for establishing chlorpyrifos reference dose. *Regul. Toxicol. Pharmacol.* **29**, 15-22.
- Clothier, B., Johnson, M.K., and Reiner, E., (1981). Interaction of some trialkyl phosphorothiolates with acetylcholinesterase: characterization of inhibition, aging and reactivation. *Biochim. Biophys. Acta* **660**, 306-316.

- Coban, A., Carr, R.L., Chambers, H.W., Willeford, K.O., and Chambers, J.E. (2016). Comparison of inhibition kinetics of several organophosphates, including some nerve agent surrogates, using human erythrocyte and rat and mouse brain acetylcholinesterase. *Toxicol. Lett.* **248**, 39-45.
- Cohen, S.D., Williams, R.A., Killinger, J.M., and Freudenthal, R.I. (1985). Comparative sensitivity of bovine and rodent acetylcholinesterase to in vitro inhibition by organophosphate insecticides. *Toxicol. Appl. Pharmacol.* **81**, 452-459.
- Cygler, M., Schrag, J.D., Sussman, J.L., Harel, M., Silman, I., Gentry, M.K., and Doctor, B.P. (1993). Relationship between sequence conservation and three-dimensional structure in a large family of esterases, lipases, and related proteins. *Protein Sci.* **2**, 366-382.
- Dodge, J.T., Mitchell, C., and Hanahan, D.J. (1963). The preparation and chemical characteristics of hemoglobin-free ghosts of human erythrocytes. *Arch. Biochem. Biophys.* **100**, 119-130.
- Dorn, M., Barbachan e Silva, M., Buriol, L.S., and Lamb, L.C. (2014). Three-dimensional protein structure prediction: methods and computational strategies. *Comp. Biol. Chem.* **53**, 251-276.
- Durst, R.A., and Staples, B.R. (1972). Tris/Tris HCl: a standard buffer for use in the physiologic pH range. *Clin. Chem.* **18**, 206-208.
- Ecobichon, D.J., and Stephens, D.S. (1973). Perinatal development of human blood esterases. *Clin. Pharmacol. Ther.* **14**, 41-47.
- Elkins, R.C., Davies, M.R., Brough, S.J., Gavaghan, D.J., Cui, Y., Abi-Gerges, N., and Mirams, G.R. (2013). Variability in high-throughput ion-channel screening data and consequences for cardiac safety assessment. *J. Pharmacol. Toxicol. Methods* **68**, 112-122.
- Ellman, G.L., Courtney, K.D., Andres, V. Jr., and Featherstone, R.M. (1961). A new and rapid colorimetric determination of acetylcholinesterase activity. *Biochem. Pharmacol.* **7**, 88-90.
- Estevez, J., and Vilanova, E. (2009). Model equations for the kinetics of covalent irreversible enzyme inhibition and spontaneous reactivation: esterases and organophosphorus compounds. *Crit. Rev. Toxicol.* **39**, 427-448.
- Exponent (2016). Update on *in vitro* acetylcholinesterase testing. Project 1508118.000 0889.
- Exponent (2017a). Update on *in vitro* acetylcholinesterase testing: amendments 1 and 2. Project 1508118.000 0889.
- Exponent (2017b). Sample size calculation or intraspecies variability in OP *in vitro* inhibition study. Memo from R. Reiss (Exponent) to N. Zinn (U.S. EPA).
- Farinde, A. (2016). Overview of pharmacodynamics. Merck Manual Professional Version. Accessed June 22, 2017. <http://www.merckmanuals.com/professional/clinical-pharmacology/pharmacodynamics/overview-of-pharmacodynamics>

- Feimlee, M.A., Morris, M.E., and Mager, D.E. (2012). Mechanism-based pharmacodynamics modeling. *Methods Mol. Biol.* **929**, 583-600.
- Fisher, S.K., and Wonnacott, S. (2012). Acetylcholine. In *Basic Neurochemistry 8<sup>th</sup> ed.* (Brady, S.T., Siegel, G.J., Albers, R.W., and Price, D.L., eds.). Elsevier, Amsterdam. pp. 258-282.
- Garcia-Lopez, J.A., and Monteoliva, M. (1988). Physiological changes in human erythrocyte cholinesterase as measured with the "pH stat". *Clin. Chem.* **34**, 2133-2135.
- Gearhart, J.M., Jepson, G.W., Clewell, H.J. III, Andersen, M.E., and Conolly, R.B. (1990). Physiologically based pharmacokinetic and pharmacodynamics model for the inhibition of acetylcholinesterase by diisopropylfluorophosphate. *Toxicol. Appl. Pharmacol.* **106**, 295-310.
- Geneious (2017). Geneious 10.2.2. Accessed June 22, 2017. <http://www.geneious.com>
- Giordano, G., and Costa, L.G. (2012). Developmental neurotoxicity: some old and new issues. *ISRN Toxicol.* **2012**, 12 pp.
- GraphPad (2018a). Confidence intervals of the EC50. *GraphPad Prism Curve Fitting Guide*. Accessed November 15, 2018. [http://www.graphpad.com/guides/prism/7/curve-fitting/index.htm?reg\\_why\\_prism\\_fits\\_the\\_logec50\\_rat.htm](http://www.graphpad.com/guides/prism/7/curve-fitting/index.htm?reg_why_prism_fits_the_logec50_rat.htm)
- GraphPad (2018b). 50% of what? Relative vs absolute IC50. Accessed November 15, 2018. <https://www.graphpad.com/support/faq/50-of-what-how-exactly-are-ic50-and-ec50-defined/>
- GraphPad (2018c). Advice: avoid Scatchard, Lineweaver-Burk and similar transforms. *GraphPad Prism Curve Fitting Guide*. Accessed November 15, 2018. [https://www.graphpad.com/guides/prism/7/curve-fitting/avoidscatchard\\_lineweaver\\_burkeandsimilartransforms.htm?toc=0&printWindow](https://www.graphpad.com/guides/prism/7/curve-fitting/avoidscatchard_lineweaver_burkeandsimilartransforms.htm?toc=0&printWindow)
- GraphPad (2018d). Equation: Michaelis-Menten model. *GraphPad Prism Curve Fitting Guide*. Accessed November 15, 2018. [https://www.graphpad.com/guides/prism/6/curve-fitting/index.htm?reg\\_michaelis\\_menten\\_enzyme.htm](https://www.graphpad.com/guides/prism/6/curve-fitting/index.htm?reg_michaelis_menten_enzyme.htm)
- Gregus, Z. (2013). Mechanisms of toxicity. In *Casarett & Doull's Toxicology: The Basic Science of Poisons 8<sup>th</sup> ed.* (Klaassen, C.D., ed.). McGraw-Hill, New York. pp. 49-122.
- Herkert, N.M., Freude, G., Kunz, U., Thiermann, H., and Worek, F. (2012). Comparative kinetics of organophosphates and oximes with erythrocyte, muscle, and brain acetylcholinesterase. *Toxicol. Lett.* **209**, 173-178.
- Herz, F., and Kaplan, E. (1973). A review: human erythrocyte acetylcholinesterase. *Pediatr. Res.* **7**, 204-214.
- Hofstee, B.H.J. (1959). Non-inverted versus inverted plots in enzyme kinetics. *Nature* **184**, 1296-1298.

- Holz, R.W., and Fisher, S.K. (2012). Synaptic transmission and cellular signaling: an overview. In *Basic Neurochemistry 8<sup>th</sup> ed.* (Brady, S.T., Siegel, G.J., Albers, R.W., and Price, D.L., eds.). Elsevier, Amsterdam. pp. 235-257.
- Karakitsos, D., and Karabinis, A. (2008). Hypothermia therapy after traumatic brain injury in children. *N. Engl. J. Med.* **359**, 1179-1180.
- Kemp, J.R., and Wallace, K.B. (1990). Molecular determinants of the species-selective inhibition of brain acetylcholinesterase. *Toxicol. Appl. Pharmacol.* **104**, 246-258.
- Kiffer, D., and Delamanche, I.S. (1983). In vitro study of organophosphorous inactivators of membrane acetylcholinesterase and of reactivating pyridinium-oximes using rat brain slices. *Biochimie* **65**, 477-483.
- Konaguthru, A.S., Whisstock, J.C., Stuckey, P.J., and Lesk, A.M. (2006). MUSTANG: a multiple structural alignment algorithm. *Proteins* **64**, 559-574.
- Kropp, T.J., and Richardson, R.J. (2003). Relative inhibitory potencies of chlorpyrifos oxon, chlorpyrifos methyl oxon, and mipafox for acetylcholinesterase versus neuropathy target esterase. *J. Toxicol. Environ. Health Part A* **66**, 1145-1157.
- Kuepfer, L., Niederal, C., Wendl, T., Willmann, S., Lippert, J., Block, M., Eissing, T., and Teutonico, D. (2016). Applied concepts in PBPK modeling: how to build a PKPL/PD model. *CPT Pharmacometrics Syst. Pharmacol.* **5**, 516-531.
- Kufareva, I., and Abagyan, R. (2012). Methods of protein structure comparison. *Meth. Mol. Biol.* **857**, 231-257.
- Le, J. (2016). Overview of pharmacokinetics. Merck Manual Professional Version. Accessed June 22, 2017. <http://www.merckmanuals.com/professional/clinical-pharmacology/pharmacokinetics/overview-of-pharmacokinetics>
- Lefkowitz, L.J., Kupina, J.M., Hirth, N.L., Henry, R.M., Noland, G.Y., Barbee, Jr., J.Y., Zhou, J.Y., and Weese, C.B. (2007). Intraindividual stability of human erythrocyte cholinesterase activity. *Clin. Chem.* **53**, 1358-1363.
- Lev-Lehman, Deutsch, V., Eldor, A., and Soreq, H. (1997). Immature human megakaryocytes produce nuclear-associated Acetylcholinesterase. *Blood* **89**, 3644-3654.
- Liang, D., Blouet, J.-P., Borrega, F., Bon, S., and Massoulié, J. (2009). Respective roles of the catalytic domains and C-terminal tail peptides in the oligomerization and secretory trafficking of human acetylcholinesterase and butyrylcholinesterase. *FEBS J.* **276**, 94-108.
- Lockridge, O., Norgren, R.B. Jr., Johnson, R.C., and Blake, T.A. (2016). Naturally occurring genetic variants of human acetylcholinesterase and butyrylcholinesterase and their potential impact on the risk of toxicity from cholinesterase inhibitors. *Chem. Res. Toxicol.* **29**, 1381-1392.

- Lovell, D.P. (2013). Biological importance and statistical significance. *J. Agric. Food Chem.* **61**, 8340-8348.
- Lowry, O.H., Rosebrough, N.J., Farr, A.L., and Randall, R.J. (1951). *J. Biol. Chem.* **193**, 265-275.
- Main, A.R. (1980). Cholinesterase inhibitors. In *Introduction to Biochemical Toxicology* (Hodgson, E., and Guthrie, F.E., eds.). Elsevier, New York. pp. 193-223.
- Martin, R.B. (1997). Disadvantages of double reciprocal plots. *J. Chem. Ed.* **74**, 1238-1240.
- Masson, P., Froment, M.-T., Sorenson, R.C., Bartels, C., and Lockridge, O. (1994). Mutation His322Asn in human acetylcholinesterase does not alter electrophoretic and catalytic properties of the erythrocyte enzyme. *Blood* **83**, 3003-3005.
- Massoulié, J. (2002). The origin of the molecular diversity and functional anchoring of cholinesterases. *Neurosignals*, **11**, 130–143.
- Massoulié, J., Perrier, N., Noureddine, H., Liang, D., and Bon, S. (2008). Old and new questions about cholinesterases. *Chem. Biol. Interact.* **175**, 30-44.
- Milatovic, D., and Dettbarn, W.-D. (1996). Modification of acetylcholinesterase during adaptation to chronic, subacute paraoxon application in rat. *Toxicol. Appl. Pharmacol.* **136**, 20-28.
- Mileson, B.E., Chambers, J.E., Chen, W.L., Dettbarn, W., Ehrich, M., Eldefrawi, A.T., Gaylor, D.W., Hamernik, K., Hodgson, E., Karczmar, A.G., Padilla, S., Pope, C.N., Richardson, R.J., Sauders, D.R., Sheets, L.P., Sultatos, L.G., and Wallace, K.B. (1998). Common mechanism of toxicity: a case study of organophosphorus pesticides. *Toxicol. Sci.* **41**, 8-20.
- Moretto, A. (1998). Experimental and clinical toxicology of anticholinesterase agents. *Toxicol. Lett.* **102-103**, 509-513.
- Mortensen, S.R., Hooper, M.J., and Padilla, S. (1998). Rat brain acetylcholinesterase activity: developmental profile and maturational sensitivity to carbamate and organophosphorus inhibitors. *Toxicology* **125**, 13-19.
- Mutch, E., and Williams, F. (2006). Diazinon, chlorpyrifos and parathion are metabolized by multiple cytochromes P450 in human liver. *Toxicology* **224**, 22-32.
- Nalivaeva, N.N., and Turner, A.J. (2001). Post-translational modifications of proteins: acetylcholinesterase as a model system. *Proteomics* **1**, 735-747.
- Navre, M. (2016). Why using pIC50 instead of IC50 will change your life. Accessed November 14, 2018. [http://cdn2.hubspot.net/hubfs/146552/docs/Why\\_Using\\_pIC50\\_will\\_Change\\_Your\\_Life.pdf?t=1443795935716](http://cdn2.hubspot.net/hubfs/146552/docs/Why_Using_pIC50_will_Change_Your_Life.pdf?t=1443795935716)
- Neal, R.A., and Halpert, J. (1982). Toxicology of thiono-sulfur compounds. *Ann Rev. Pharmacol. Toxicol.* **22**, 321-339.

- Needham, L.L. (1994). Examples of measuring internal dose for assessing exposure in epidemiological studies. In *Environmental Epidemiology: Effects of Chemicals on Human Health* (Draper, W.M., ed.). American Chemical Society, Washington, DC. pp. 121-135.
- NRC (2009). *Science and Decisions: Advancing Risk Assessment*. National Academies Press, Washington, DC. 403 pp.
- O'Brien, R.D. (1968). Kinetics of the carbamylation of cholinesterase. *Mol. Pharmacol.* **4**, 121-130.
- Ochs, R.S. (2010). The problem with double reciprocal plots. *Curr. Enz. Inhib.* **6**, 164-169.
- Ordentlich, A., Barak, D., Kronman, C., Ariel, N., Segall, Y., Velan, B., and Shafferman, A. (1996). The architecture of human acetylcholinesterase active center probed by interactions with selected organophosphate inhibitors. *J. Biol. Chem.* **271**, 11953-11962.
- Pavlic M (1967) The inhibitory effect of TRIS on the activity of cholinesterases. *Biochim. Biophys. Acta* **139**, 133–13.
- PDB (2017a). 5FPQ: Structure of homo sapiens acetylcholinesterase phosphorylated by sarin. Accessed June 23, 2017. <http://www.rcsb.org/pdb/explore/explore.do?structureId=5fpq>
- PDB (2017b). 2Y2V: Nonaged form of mouse acetylcholinesterase inhibited by sarin -- update. Accessed June 23, 2017. <http://www.rcsb.org/pdb/explore/explore.do?structureId=2y2v>
- Richardson, R.J. (1992). Interactions of organophosphorus compounds with neurotoxic esterase. In *Organophosphates: Chemistry, Fate, and Effects*. (Chambers, J.E., and Levi, P.E., eds.). Academic Press, San Diego. pp. 299-323.
- Richardson, R.J. (2010). Anticholinesterase insecticides. In *Comprehensive Toxicology*, vol. 13 (McQueen, C.A., ed.). Oxford: Academic Press, pp. 433-444.
- Richardson, R.J., Worden, R.M., Wijeyesakere, S.J. Hein, N.D., Fink, J.K., and Makhaeva, G.F. (2015). Neuropathy target esterase as a biomarker and biosensor of delayed neuropathic agents. In *Handbook of Toxicology of Chemical Warfare Agents*, 2<sup>nd</sup> ed. (Gupta, R.C., ed.). Elsevier, Amsterdam. pp. 935-952.
- Ritchie, R.J., and Prvan, T. (1996). Current statistical methods for estimating the  $K_m$  and  $V_{max}$  of Michaelis-Menten kinetics *Biochem. Edu.* **24**, 196-206.
- Rumenjak, V. (1998). Distribution of human erythrocyte acetylcholinesterase according to age, sex and pregnancy. *Acta Med. Croatia* **52**, 187-189.
- Sharp, P., and Villano, J.S. (2012). *The Laboratory Rat*, 2nd ed. CRC Press, Boca Raton, FL, p. 106.
- Spinedi, A., Pacini, L., and Lulu, P. (1989). A study of the mechanism by which some amphiphilic drugs affect human erythrocyte acetylcholinesterase activity. *Biochem. J.* **261**, 569-573.

- Spinedi, A., Luly, P., and Farias, R.N. (1993). Does the fluidity of the lipid environment modulate membrane-bound acetylcholinesterase? Effects of temperature, membrane composition and amphiphiles. *Biochem. Pharmacol.* **46**, 1521-1527.
- Strelow, J.M. (2017). A perspective on the kinetics of covalent and irreversible inhibition. *SLAS Discov.* **22**, 3-20.
- Taylor, P., Li, Y., Camp, S., Rachinsky, T.L., Ekstrom, T., Getman, D., Fuentes, M.E., Vellom, D.C., and Radic, Z. (1993). Structure and regulation of expression of the acetylcholinesterase gene. *Chem. Biol. Interact.* **87**, 199-207.
- Thompson, C.M., and Richardson, R.J. (2004). Anticholinesterase insecticides. In *Pesticide Toxicology and International Regulation* (Marrs, T.C., and Ballantyne, B., eds.). John Wiley & Sons, Ltd., Chichester, England. pp. 89-127.
- Uniprot (2017a). P22303 (ACES\_HUMAN). Accessed June 22, 2017. <http://www.uniprot.org/uniprot/P22303>.
- Uniprot (2017b). P37136 (ACES\_RAT). Accessed June 22, 2017. <http://www.uniprot.org/uniprot/P37136>
- Uniprot (2017c). P21836 (ACES\_MOUSE). Accessed June 23, 2017. <http://www.uniprot.org/uniprot/P21836>
- U.S. EPA (2000). The Use of Data on Cholinesterase Inhibition for Risk Assessments of Organophosphorus and Carbamate Pesticides. USEPA, Washington, DC. 51 pp.
- U.S. EPA (2002a). Guidance on Cumulative Risk Assessment of Pesticide Chemicals that have a Common Mechanism of Toxicity. USEPA, Washington, DC. 81pp.
- U.S. EPA (2002b). Revised OP (Organophosphate) Cumulative Risk Assessment. Accessed June 22, 2017. <https://nepis.epa.gov/Exe/ZyPDF.cgi/9100BFL.L.PDF?Dockey=9100BFL.L.PDF>. 28 pp.
- U.S. EPA (2002c). A Review of the Reference Dose and Reference Concentration Processes. USEPA, Washington, DC. 192 pp.
- U.S. EPA (2006). Approaches for the application of physiologically based pharmacokinetic (PBPK) models and supporting data in risk assessment. USEPA, Washington, DC. 123 pp.
- U.S. EPA (2014). Guidance for Applying Quantitative Data to Develop Data-Derived Extrapolation Factors for Interspecies and Intraspecies Extrapolation. U.S. EPA, Washington, DC. 109 pp.
- U.S. EPA (2016a). Review of a Protocol for *In Vitro* Acetylcholinesterase Testing with Several OP Chemicals. DP Barcode D436127.
- U.S. EPA (2016b). Malathion: Human Health Draft Risk Assessment for Registration Review. DP Barcode D414107.



- Valle, A.M., Radic, Z., Rana, B.K., Mahboubi, V., Wessel, J., Shih, P.B., Rao, R., O'Connor, D.T., and Taylor, P. (2011). Naturally occurring variations in the human cholinesterase genes: heritability and association with cardiovascular and metabolic traits. *J. Pharm. Exp. Ther.* **338**, 125-133.
- Velan, B., Grosfeld, H., Kronman, C., Leitner, M., Gozes, Y., Lazar, A., Flashner, Y., Marcus, D., Cohen, S., and Shafferman, A. (1991). The effect of elimination of intersubunit disulfide bonds on the activity, assembly, and secretion of recombinant human acetylcholinesterase. Expression of acetylcholinesterase Cys580-Ala mutant. *J. Biol. Chem.* **266**, 23977-23984.
- Velan, B., Kronman, C., Ordentlich, A., Flashner, Y., Leitner, M., Cohen, S., and Shafferman, A. (1993). N-glycosylation of human acetylcholinesterase: effects on activity, stability, and biosynthesis. *Biochem. J.* **286**, 649-656.
- Vidair, C.A. (2004). Age dependence of organophosphate and carbamate neurotoxicity in the postnatal rat: extrapolation to the human. *Toxicol. Appl. Pharmacol.* **196**, 287-302.
- Voicu, V.A., Thiermann, H., Radulescu, F.S., Mircioiu, C., and Miron, D.S. (2009). The toxicokinetics and toxicodynamics of organophosphonates versus the pharmacokinetics and pharmacodynamics of oxime antidotes: biological consequences. *Basic Clin. Pharmacol. Toxicol.* **106**, 73-85.
- Wiener, N., and Taylor, P. (1985). Neurohumoral transmission: the autonomic and somatic motor nervous systems. In *Goodman and Gilman's The Pharmacological Basis of Therapeutics, 7<sup>th</sup> ed.* (Gilman, A.G., Goodman, L.S., Rall, T.W., and Murad, F., eds.). Macmillan, New York. pp. 66-109.
- Wiesner, J., Zdenek, K., Kuca, K., Jun, D., and Koca, J. (2007). Acetylcholinesterases – the structural similarities and differences. *J. Enz. Inhib. Med. Chem.* **22**, 417-424.
- Wilkinson, G.N. (1961). Statistical estimations in enzyme kinetics. *Biochem. J.* **80**, 324-332.
- Wille, T., Thiermann, H., and Worek, F. (2011). Effect of different buffers on kinetic properties of human acetylcholinesterase and the interaction with organophosphates and oximes. *Arch. Toxicol.* **85**, 193-198.
- Worek, F., Aurbek, N., Wetherell, J., Pearce, P., Mann, T., and Thiermann, H. (2008). Inhibition, reactivation and aging kinetics of highly toxic organophosphorus compounds: pig versus minipig acetylcholinesterase. *Toxicology* **244**, 35-41.
- Worek, F., Aurbek, N., Wille, T., Eyer, P., and Thiermann, H. (2011). Kinetic analysis of interactions of paraoxon and oximes with human, Rhesus monkey, swine, rabbit, rat and guinea pig acetylcholinesterase. *Toxicol. Lett.* **200**, 19-23.
- Xie, W., Stribley, J.A., Chatonnet, A., Wilder, P.J., Rizzino, A., McComb, R.D., Taylor, P., Hinrichs, S.H., and Lockridge, O. (2000). Postnatal developmental delay and supersensitivity to organophosphate in gene-targeted mice lacking acetylcholinesterase. *J. Pharmacol. Exp. Ther.* **293**, 896-902.
- YASARA (2017). YASARA-Structure 17.4.17. Accessed June 22, 2017. <http://www.yasara.org>

Zierler, K. (1977). An error in interpretation of double-reciprocal plots and Scatchard plots in studies of binding of fluorescent probes to proteins, and alternative proposals for finding binding parameters. *Biophys. Struct. Mech.* **3**, 275-289.

Zimmermann, M. (2013). Neuronal AChE splice variants and their non-hydrolytic functions: redefining a target of AChE inhibitors? *Br. J. Pharmacol.* **170**, 953-967.

## Appendix A – List of OP Compounds in the Experimental Program\*

---

1. Naled
2. DDVP
3. Dicrotophos
4. Tribufos
5. Terbufos oxon sulfoxide
6. Terbufos oxon sulfone
7. Chlorethoxyfos oxon
8. Tebupirimphos oxon
9. Phorate oxon sulfoxide
10. Phorate oxon sulfone
11. Ethoprop
12. Methamidophos
13. Fenamiphos
14. Malaaxon
15. Dimethoate
16. Bensulide oxon
17. Phosmet oxon

\*In addition to the reference compound, parao